

Simultaneous constraints on the growth of structure and cosmic expansion from the multipole power spectra of the SDSS DR7 LRG sample

Akira Oka^{1*}, Shun Saito², Takahiro Nishimichi³, Atsushi Taruya^{2,4,5},
Kazuhiro Yamamoto⁶

¹ Department of Physics, University of Tokyo, Tokyo 113-0033, Japan

² Kavli Institute for the Physics and Mathematics of the Universe (WPI), University of Tokyo, Chiba 277-8583, Japan

³ Institut d'Astrophysique de Paris, CNRS, 98 bis Boulevard Arago, F-75014 Paris, France

⁴ Research Center for the Early Universe, School of Science, University of Tokyo, Tokyo 113-0033, Japan

⁵ Yukawa Institute for Theoretical Physics, Kyoto University, Kyoto 606-8502, Japan

⁶ Department of Physical Science, Hiroshima University, Higashi-Hiroshima 739-8526, Japan

12 July 2018

ABSTRACT

The anisotropic galaxy clustering on large scales provides us with a unique opportunity to probe into the gravity theory through the redshift-space distortions (RSDs) and the Alcock-Paczynski effect. Using the multipole power spectra up to hexadecapole ($\ell = 4$), of the Luminous Red Galaxy (LRG) sample in the data release 7 (DR7) of the Sloan Digital Sky Survey II (SDSS-II), we obtain simultaneous constraints on the linear growth rate f , angular diameter distance D_A , and Hubble parameter H at redshift $z = 0.3$. For this purpose, we first extensively examine the validity of a theoretical model for the non-linear RSDs using mock subhalo catalogues from N -body simulations, which are constructed to match with the observed multipole power spectra. We show that the input cosmological parameters of the simulations can be recovered well within the error bars by comparing the multipole power spectra of our theoretical model and those of the mock subhalo catalogues. We also carefully examine systematic uncertainties in our analysis by testing the dependence on prior assumption of the theoretical model and the range of wavenumbers to be used in the fitting. These investigations validate that the theoretical model can be safely applied to the real data. Thus, our results from the SDSS DR7 LRG sample are robust including systematics of theoretical modeling; $f(z = 0.3)\sigma_8(z = 0.3) = 0.49 \pm_{stat.} 0.08 \pm_{sys.} 0.04$, $D_A(z = 0.3) = 968 \pm_{stat.} 42 \pm_{sys.} 17$ [Mpc], $H(z = 0.3) = 81.7 \pm_{stat.} 5.0 \pm_{sys.} 3.7$ [km/s/Mpc]. We believe that our method to constrain the cosmological parameters using subhaloes catalogues will be useful for more refined samples like CMASS and LOWZ catalogues in the Baryon Oscillation Spectroscopic Survey in SDSS-III.

Key words: cosmology: large-scale structure of Universe, cosmological parameters, galaxies: haloes, statistics

1 INTRODUCTION

Cosmic acceleration is strongly supported by a recent set of cosmological observations including the cosmic microwave background (CMB) anisotropies (Hinshaw et al. 2012; Planck Collaboration 2013) and Type Ia supernovae (Riess et al. 1998; Perlmutter et al. 1999; Suzuki et al. 2012). Revealing the origin of the cosmic acceleration is one of the

key sciences in modern physics, and there are therefore ongoing or planned cosmological observations from various points of view (for a recent review, see Weinberg et al. (2013)). The origin of cosmic acceleration may be explained by either of two possible ways as follows. One is to introduce mysterious energy component with negative pressure, the so-called dark energy. Another is to modify general relativity on infra-red scales while keeping unchanged on small scales so that the theory can pass tests of gravity in the solar system. It is desirable to establish a methodology to distinguish two possibilities and even to identify the nature of dark energy or

* E-mail: oka@utap.phys.s.u-tokyo.ac.jp

the theory of gravity on cosmological scales (for a review of modified gravity, see Jain & Khoury (2010)).

A standard approach to tackle this problem is to combine measurements of the expansion history with those of the growth of the large-scale structure at different time and scales. Interestingly, the clustering of galaxies at large scales provides us with a unique opportunity to simultaneously measure both probes. There are various completed, ongoing or proposed galaxy redshift surveys which include the 2dF Galaxy Redshift Survey (2dFGRS) (Colless et al. 2001), Sloan Digital Sky Survey (SDSS) (for the latest data release (DR), see Ahn et al. (2013)), WiggleZ dark energy survey (Blake et al. 2009a), Subaru Prime Focus Spectrograph (PFS) Survey (Ellis et al. 2012), Dark Energy Spectroscopic Instrument (DESI) (Levi et al. 2013) and Euclid (Laureijs et al. 2011). Most of such gigantic galaxy redshift surveys are designed to detect the baryon acoustic oscillation (BAO) scale that is used as a standard ruler to explore the expansion history (Anderson et al. 2012; Beutler et al. 2011; Blake et al. 2011c; Eisenstein et al. 2005b; Percival et al. 2007a; Seo et al. 2012).

While the BAO scale is usually measured from the isotropic or the spherically-averaged part of the clustering signal, in this paper we focus on the anisotropic part which in fact carries additional information on the cosmic growth and expansion history. The anisotropies on the galaxy clustering arise from two effects: The first one is the Alcock-Paczynski (AP) effect (Alcock & Paczynski 1979). This effect arises if the background expansion of the real universe differs from the fiducial cosmology when converting the observed galaxy positions, i.e., redshift and angular positions, to the comoving radial and transverse distances. The measured clustering pattern in distance space is distorted in a purely geometrical way through this effect. The distortion perpendicular to line of sight is proportional to the angular diameter distance, $D_A(z)$, while one parallel to the line of sight is inversely proportional to the Hubble parameter, $H(z)$, evaluated with the assumed fiducial cosmology (Matsubara & Suto 1996; Ballinger et al. 1996; Padmanabhan & White 2008). Thus, using the BAO signature imprinted on the galaxy clustering as a standard ruler, these distortions can be measured, leading to a precise determination of $D_A(z)$ and $H(z)$ (e.g. Matsubara 2004e; Seo & Eisenstein 2003). The second effect is the redshift-space distortions (RSDs) caused by peculiar velocities of galaxies (e.g. Hamilton 1998b; Peebles 1980). Since again the radial positions of galaxies are determined by their redshifts, the radial positions in redshift space are contaminated by their peculiar velocities along the line-of-sight direction. Thus, RSDs makes the line-of-sight direction special, also inducing anisotropies in the apparent clustering. In other words, RSDs allow us to extract information on the velocity field through a measurement of anisotropies, which can be used as a powerful probe of modified gravity because the velocity field is related to the Newton potential via the Euler equation (Guzzo et al. 2008; Yamamoto et al. 2008c). In the linear theory of density perturbations, RSDs are characterized by the linear growth rate defined by $f \equiv d \ln D_+(a) / d \ln a$, where $D_+(a)$ is the linear growth factor. Note that this dynamical measure from RSDs is complementary to weak lensing analyses or the measurements of the integrated Sachs-Wolfe effect in

CMB anisotropies which probes the sum of two gravitational potentials (e.g. Bertschinger (2006); Kimura et al. (2012)).

While RSDs are qualitatively understood as a combination of the squashing effect on large scales, known as the Kaiser effect (Sargent & Turner 1977; Kaiser 1987), and the so-called Finger-of-God (FoG) dilution effect at small scale (Jackson 1972), it is challenging to accurately model the galaxy clustering at intermediate regime where non-linearity of the structure formation cannot be negligible (for a review, see Bernardeau et al. (2002)). The difficulty here is the non-linear mapping from real space to redshift space, and various efforts have recently been made for the accurate prediction of the power spectrum or the correlation function in redshift space on the basis of perturbative approaches (Matsubara 2008c,b, 2011d, 2013a; Nishimichi & Taruya 2011; Okumura et al. 2012b,a; Reid & White 2011; Scoccimarro 2004a; Seljak & McDonald 2011; Taruya et al. 2009c, 2010d, 2013a; Vlah et al. 2012b, 2013a; Wang et al. 2013). Though such previous works show a successful performance for the clustering of dark matter or dark matter haloes when compared with N -body simulations, it is still necessary to validate such an approach using more realistic galaxy mock catalogues.

The main goal of this paper is to simultaneously obtain robust constraints on f , D_A , and H from the anisotropic galaxy power spectrum. As a specific example, we are going to use the luminous red galaxy (LRG) sample in SDSS-II DR7 (Abazajian et al. 2009; Eisenstein et al. 2001a). Even though more recent samples such as CMASS and LOWZ from Baryon Oscillation Spectroscopic Survey (BOSS) in SDSS-III DR10 are publicly available (Ahn et al. 2013), it is still interesting to investigate the anisotropic clustering signal in the DR7 LRG sample for following reasons. First of all, DR7 LRG is one of the samples with which the multipole power spectra are properly measured (Hikage & Yamamoto 2013; Yamamoto et al. 2008c, 2010b) with reasonable precisions, while some attempts have been made in the literature (Blake et al. 2011b; Cole et al. 1994a; Hamilton 1995a; Hatton & Cole 1999). In order to measure the redshift-space distortions in the anisotropic distribution of galaxies, it is useful to expand the anisotropic power spectrum into the sum of the Legendre polynomials. Note also that the significance of the survey window effect in the DR7 LRG catalogue has been discussed in (Sato et al. 2013a, 2011b).

As briefly explained in Section 2, measuring the multipole power spectra, is not straightforward. Although one usually assumes a fixed line-of-sight direction in order to utilize the fast-Fourier transformation (FFT), Yoo & Seljak (2013) (and its references therein) shows that this assumption is not appropriate to interpret the large-scale anisotropies especially for surveys covering wide sky area such as the SDSS. Secondly, a couple of previous works addressed the anisotropic signal of LRGs via the correlation function (Samushia et al. 2012; Xu et al. 2013), but they did not consider a simultaneous constraint on f , D_A and H via the AP effect and RSDs. As shown in Taruya et al. (2011e), the results could be biased if one of them is artificially fixed since there must be moderate degeneracies among f , D_A and H . Note that Reid et al. (2012a) present such a simultaneous constraint using the DR9 CMASS sample (see also Chuang & Wang (2012a, 2013b,c); Hemantha et al. (2013) for similar attempts with the DR7 LRGs).

Another reason why there is still room to explore the

LRG sample is that no work has tested the validity of the methodology to extract the anisotropic signal against a ‘realistic’ mock catalogue. In particular, the FoG effect due to satellite galaxies is worrisome even on large scales. Studies with high-resolution simulations on dark matter haloes and subhaloes suggest a division of galaxies into central and satellite galaxies (e.g. see Kravtsov et al. (2004)). The halo occupation distribution (HOD) model (for a review, see Cooray & Sheth (2002)) is a useful tool to describe the link between galaxies and dark matter. Detailed HOD studies via the small-scale clustering show that a majority of LRGs is considered as central while roughly $\sim 5\%$ of LRGs is satellite surrounding central galaxy (Zheng et al. 2008; Reid & Spergel 2009). Since satellites have intrahalo velocities causing the FoG effect, it is important to include the effect of satellites into the theoretical model when one analyses the anisotropic clustering on smaller scales beyond the limitation of perturbation theory (PT) (Hikage & Yamamoto 2013). Note that even off-centred central galaxy may also result in additional FoG effect (Hikage et al. 2012b,a). Our companion paper shows that a properly-chosen *subhalo* catalogue is able to resemble such two populations of LRGs and indeed reproduce the measured multipole power spectra (Nishimichi & Oka 2013). While most of studies with subhaloes are explored in the context of subhalo abundance matching, called as the SHAM (e.g. Conroy et al. (2006); Masaki et al. (2012)), our subhalo catalogue is based on a simple mass cut so that it reproduces the measured anisotropic signal and hence complementary to the SHAM scheme.

In this work, we extensively and systematically study our RSD model against such a realistic mock catalogue. We adopt the PT-based model for non-linear RSDs developed by Taruya et al. (2010d). We then combine it with a simple but phenomenological function for linear and scale-dependent galaxy bias, motivated by Nishimichi & Taruya (2011) (see also Ishikawa et al. (2013) for a similar approach). After systematically studying the validity of our approach, we will present simultaneous constraints on f , D_A , and H from the DR7 LRG sample.

This paper is organized as follows: Section 2 is devoted to explain the data set we analyse, namely, the monopole, quadrupole, and hexadecapole power spectra of the LRG sample in SDSS DR7. In Section 3, we introduce the theoretical model of the multipole power spectra to face with the observation. The validity of our analysis is tested against the mock catalogue in Section 4. The results of our analysis with the real data set of the DR7 LRG sample are presented and compared with several previous studies in Section 5. Finally, we summarize this work in Section 6.

2 POWER SPECTRUM MEASUREMENT

In this section, we briefly summarize the measurement of the multipole power spectra of LRGs in the SDSS DR7 (Abazajian et al. 2009). We use the same data set as in (Yamamoto et al. 2010b). The DR7 LRG sample is selected to cover the redshift range, $0.16 < z < 0.47$, only in the northern cap in order to reduce systematics uncertainties. Thus, the sky coverage is limited to $\sim 7,150 \text{ deg}^2$ and the total number of LRGs is $N_{\text{LRG}} = 100,157$. This corresponds to a sur-

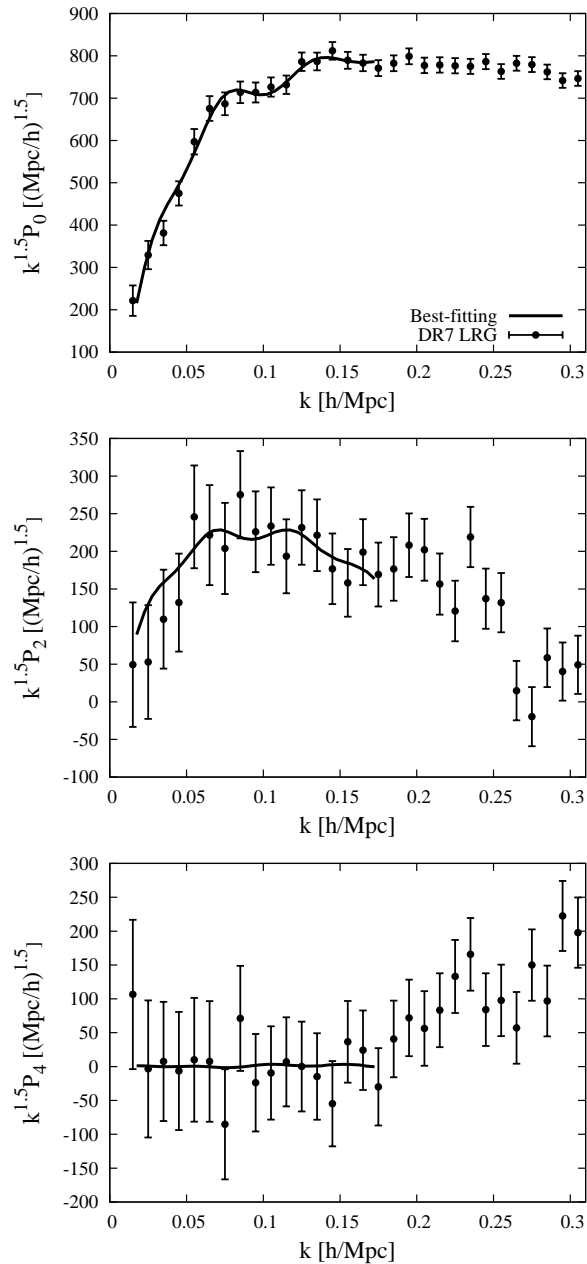


Figure 1. The filled circles with error bars are the observed multipole spectra, monopole (top), quadrupole (middle), and hexadecapole (bottom) power spectra of the SDSS DR7 LRG sample. We plot the best-fitting results with solid curves, whose details are described in Section 5. The results are multiplied by $k^{1.5}$. The best-fitting curves are plotted in the range of the wavenumbers $k \leq k_{\text{max}} = 0.175[h/\text{Mpc}]$ that corresponds to the valid range of our theoretical model (see Section 4.3). We used the data in the range of the wavenumbers $k \leq k_{\text{max}} = 0.175[h/\text{Mpc}]$, which include 51 data points, as described in Section 5.

vey volume of $V_{\text{survey}} \sim 1.3 [\text{Gpc}^3/h^3]$. We adopt the same method for the measurement as in (Yamamoto et al. 2010b, 2006a) but with the fiducial cosmological background favored by the Planck results (Planck Collaboration 2013). Namely, we adopt the distant-redshift relation of the spatially flat ΛCDM cosmology with $\Omega_m = 0.32$, $h = 0.67$.

In our algorithm, the line-of-sight direction is chosen

for each pair of galaxies, which enables us to measure the higher multipole spectra without introducing the fixed line-of-sight direction. With this algorithm, the window effect can be kept small for the SDSS DR7 LRG sample, which we neglect in the present paper (Sato et al. 2011b).

The multipole power spectra, $P_\ell(k)$, are the coefficients of the Legendre multipole expansion of the anisotropic power spectrum,

$$P^s(k, \mu) = \sum_{\ell=\text{even}} P_\ell(k) \mathcal{L}_\ell(\mu), \quad (1)$$

$$P_\ell(k) = \frac{2\ell+1}{2} \int_{-1}^1 d\mu \mathcal{L}_\ell(\mu) P^s(k, \mu), \quad (2)$$

where $\mathcal{L}_\ell(\mu)$ is the ℓ -th Legendre polynomial, and μ is the directional cosine between the line-of-sight direction and the wavenumber vector. The anisotropic power spectrum is useful to constrain both the cosmic expansion history and the growth history of the large scale structure of the universe. In the present paper, we demonstrate the cosmological constraints from the combination of the monopole, quadrupole, and hexadecapole power spectra, $P_0(k)$, $P_2(k)$, and $P_4(k)$, which provide almost as much information on f , D_A , and H as the full two-dimensional anisotropic power spectrum as long as one restricts the analysis within the valid range of perturbative approaches (Taruya et al. 2011e).

In our measurement of the multipole power spectra, we adopt an estimator, $\hat{P}_\ell(k)$, for discrete density fields (Yamamoto et al. 2006a):

$$\hat{P}_\ell(k) = \frac{2\ell+1}{\Delta V_k} \int_{\Delta V_k} d^3k \{R_\ell(\mathbf{k}) - S_\ell(\mathbf{k})\}, \quad (3)$$

where ΔV_k is the volume of a shell in the Fourier space, R_ℓ and S_ℓ , are defined by

$$R_\ell(\mathbf{k}) = A^{-1} \left[\sum_{i_1}^{N_{\text{LRG}}} e^{i\mathbf{k}\cdot\mathbf{s}_{i_1}} \mathcal{L}_\ell(\mu_{i_1}) - \gamma \sum_{j_1}^{N_{\text{rand}}} e^{i\mathbf{k}\cdot\mathbf{s}_{j_1}} \mathcal{L}_\ell(\mu_{j_1}) \right] \\ \times \left[\sum_{i_2}^{N_{\text{LRG}}} e^{i\mathbf{k}\cdot\mathbf{s}_{i_2}} - \gamma \sum_{j_2}^{N_{\text{rand}}} e^{i\mathbf{k}\cdot\mathbf{s}_{j_2}} \right], \quad (4)$$

$$S_\ell(\mathbf{k}) = A^{-1} (1 + \gamma) \sum_i^{N_{\text{LRG}}} \mathcal{L}_\ell(\mu_i), \quad (5)$$

where \mathbf{s}_i and \mathbf{s}_j are positions of galaxies and of random samples in redshift space, respectively, $\gamma = N_{\text{LRG}}/N_{\text{rand}}$, is the ratio of the number of LRGs to that of random samples, for which we set $\gamma = 0.05$, and $\mu = \mathbf{k} \cdot \mathbf{s}/|\mathbf{k}||\mathbf{s}|$. Here A is defined by the integration of the mean number density over observed redshift,

$$A = \Delta\Omega \int_{s(z_{\text{min}})}^{s(z_{\text{max}})} ds s^2 \bar{n}^2(z), \quad (6)$$

where s is the radial (comoving) coordinate of the fiducial cosmological background, and $\Delta\Omega$ is the solid angle of the survey area.

The statistical error of the multipole power spectra may be estimated by the formula in (Yamamoto et al. 2006a).

Adopting the constant weight factor, we have

$$\Delta \hat{P}_\ell(k)^2 = 2(2\ell+1)^2 \frac{(2\pi)^3}{\Delta V_k^2} \int_{\Delta V_k} d^3k \frac{1}{A^2} \\ \times \int_{s(z_{\text{min}})}^{s(z_{\text{max}})} ds \bar{n}^4(z) \left[P(\mathbf{k}, \mathbf{s}) + \frac{1}{\bar{n}(\mathbf{s})} \right]^2 \mathcal{L}_\ell^2(\hat{\mathbf{s}} \cdot \hat{\mathbf{k}}), \quad (7)$$

where we used the approximation $P(\mathbf{k}, \mathbf{s}) \simeq P_0(k) + P_2(k) \mathcal{L}_2(\hat{\mathbf{s}} \cdot \hat{\mathbf{k}})$, which has been derived on the basis of the so-called FKP method (Feldman et al. 1994).

This estimation of the statistical error is not strict but rather optimistic in the following points. First, covariances between different ℓ -th multipoles are neglected. Second, covariances between different k -bins, i.e., the non-Gaussian error, from the window effect and the non-linear gravitational growth are not taken into account. Our cosmological parameter estimation in the following sections is slightly altered when the covariances between different ℓ - and k -bins are properly taken into account, which are obtained in (Sato et al. 2013a, 2011b). However, the effect of such non-Gaussian error on the resultant one-dimensional marginalized errors is small, as shown in Takahashi et al. (2009, 2011b). Therefore we will consider only the diagonal component of the covariance matrix for simplicity from now on.

Figure 1 demonstrates the resultant multipole power spectra, the monopole (top), quadrupole (middle), and hexadecapole (bottom), respectively. The solid curves in each panel show the best-fitting results described in Section 5.

3 MODELING THE MULTIPOLE POWER SPECTRA

In this section, we briefly review the theoretical model of the multipole power spectra used in the cosmological analysis. Our goal is to constrain the linear growth rate and geometrical factors simultaneously through RSDs and AP effect in an unbiased manner. For this purpose, a proper modeling of the shape and the amplitude of the anisotropic power spectrum is rather crucial (e.g. Padmanabhan & White (2008)), and we will investigate the robustness of our model in detail in Section 4. The model presented here is based on the perturbation theory calculation, and we will separately give prescription on how to compute the multipole power spectra.

3.1 Redshift-space distortions and Non-linear gravitational growth

Redshift-space distortions and gravitational clustering involve, in nature, non-linear and non-Gaussian effects, and it is quite essential to take a proper account of these for a robust cosmological analysis beyond the linear scales. Since we are interested in a large-scale anisotropic clustering at moderately high redshift, the PT approach should work well, and a percent-level precision is achievable with PT calculation in weakly non-linear regime $k \lesssim 0.2 [h/\text{Mpc}]$.

Let us first consider RSDs. It is well-known that the clustering statistics in redshift space are influenced by the two effects, the Kaiser and Finger-of-God effects. While the former comes from the coherent motion of galaxies and enhances the clustering amplitude, the latter is mainly attributed to the virialized random motion of galaxies sitting

in a halo and suppresses the power spectrum significantly along the line of sight. Strictly speaking, these effects cannot be treated separately, and through the higher-order corrections, a tight correlation between the density and velocity fields still plays an important role on the scales of our interest. In the present paper, among several proposed models to account for the non-linear RSDs ((Matsubara 2008b; Reid & White 2011; Seljak & McDonald 2011)), we adopt the model given by (Taruya et al. 2010d) (hereafter, TNS model):

$$P^s(k, \mu) = D_{\text{FoG}}(k\mu f\sigma_v) \times \left[P_{\text{Kaiser}}(k, \mu; f) + A(k, \mu; f) + B(k, \mu; f) \right], \quad (8)$$

where σ_v is a nuisance parameter, which is related to the one-dimensional velocity dispersion. The function $D_{\text{FoG}}(k\mu f\sigma_v)$ characterizes the suppression of the power spectrum by the FoG effect, for which we adopt the Gaussian form;

$$D_{\text{FoG}}(x) = \exp(-x^2). \quad (9)$$

The function, $P_{\text{Kaiser}}(k, \mu)$, is the non-linear generalization of the Kaiser term given by (Scoccimarro 2004a)

$$P_{\text{Kaiser}}(k, \mu; f) = P_{\delta\delta}(k) + 2f\mu^2 P_{\delta\theta}(k) + f^2\mu^4 P_{\theta\theta}(k). \quad (10)$$

Here, the functions $P_{\delta\delta}(k)$, $P_{\theta\theta}(k)$, and $P_{\delta\theta}(k)$ are respectively the auto-power spectra of the density and the velocity divergence, and their cross-power spectrum. Here, the velocity divergence, θ , is normalized as $\theta \equiv -\nabla_{\mathbf{v}}/(faH)$.

The main characteristic of the model (8) is the two additional terms A and B , which represent the higher-order coupling between the velocity and density fields, usually ignored in a phenomenological model of RSDs. These corrections have been properly derived on the basis of the low- k expansion from the exact expression of the anisotropic power spectrum, expressed as

$$A(k, \mu; f) = (k\mu f) \int \frac{d^3\mathbf{p}}{(2\pi)^3} \frac{p_z}{p^2} \times \left[B_{\sigma}(\mathbf{p}, \mathbf{k} - \mathbf{p}, -\mathbf{k}) - B_{\sigma}(\mathbf{p}, \mathbf{k}, -\mathbf{k} - \mathbf{p}) \right], \quad (11)$$

$$B(k, \mu; f) = (k\mu f)^2 \int \frac{d^3\mathbf{p}}{(2\pi)^3} F(\mathbf{p})F(\mathbf{k} - \mathbf{p});$$

$$F(\mathbf{p}) = \frac{p_z}{p^2} \left[P_{\delta\theta} + f \frac{p_z^2}{p^2} P_{\theta\theta} \right], \quad (12)$$

where the function, $B_{\sigma}(\mathbf{k}_1, \mathbf{k}_2, \mathbf{k}_3)$, is the cross bispectrum defined by

$$(2\pi)^3 \delta_{\text{D}}(\mathbf{k}_1 + \mathbf{k}_2 + \mathbf{k}_3) B_{\sigma}(\mathbf{k}_1, \mathbf{k}_2, \mathbf{k}_3) = \left\langle \theta(\mathbf{k}_1) \left[\delta(\mathbf{k}_2) + f \frac{k_{2z}^2}{k_2^2} \theta(\mathbf{k}_2) \right] \left[\delta(\mathbf{k}_3) + f \frac{k_{3z}^2}{k_3^2} \theta(\mathbf{k}_3) \right] \right\rangle. \quad (13)$$

It is shown in the previous study that these two terms enhance the amplitude of the power spectrum over the wavenumbers where the baryon acoustic feature is prominent, and moderately but notably change the acoustic structure imprinted on the power spectrum (Taruya et al. 2010d). As a result, the model (8) successfully describes both the matter and halo power spectra of N -body simulations at weakly non-linear scales. In particular, the non-Gaussian contribution described by A term exhibits a strong dependence on halo/galaxy biasing, and in addition to the linear

Kaiser effect, it gives a rather prominent enhancement in the multipole power spectra (Nishimichi & Taruya 2011). Since the effect is known to be significant for highly biased objects, the model (8) seems best suited for characterizing the anisotropic LRG clustering in weakly non-linear regime.

To compute the power spectrum (8), we need to further incorporate the effect of non-linear gravitational growth into each term. In this paper, we apply the resummed PT scheme called **RegPT** (Taruya et al. 2012f), and following the prescription described in (Taruya et al. 2013a), we evaluate the power spectrum and bispectrum contributions, consistently including the non-linear corrections up to the two-loop order, i.e., next-to-next-leading order. The **RegPT** scheme is based on the multipoint propagator expansion, in which non-perturbative properties of gravitational growth are wholly encapsulated. With this scheme, any statistical quantities consisting of the density and velocity fields are built up with the multipoint propagators. Making use of the analytic properties of the propagators, a novel regularized treatment has been implemented, which allows us to consistently reproduce the standard PT results at low- k and the expected resummed behavior at high- k . It has been demonstrated that the proposed scheme can be used to give a percent-level prediction of the power spectrum and the correlation function at weakly non-linear regime in both real and redshift spaces (Taruya et al. 2012f, 2013a). At redshift $z \simeq 0.3$, while the standard PT fails to reproduce the matter power spectrum at $k \sim 0.1$ [h/Mpc], the applicable range of **RegPT** is rather wider, and it can cover the almost entire scales of BAOs.

3.2 Galaxy bias

With the **RegPT** scheme, the model (8) can give us an accurate prediction for the multipole power spectra with its applicable range much beyond linear scales. Note, however, that the aforementioned model has been originally proposed for the matter distribution, and a proper account of the galaxy bias is necessary for a cosmological analysis with the DR7 LRG sample. While there have been several sophisticated PT schemes proposed to simultaneously characterize the galaxy bias, redshift-space distortions, and non-linear gravitational growth, we here adopt a rather simple approach. Namely, we assume a linear bias relation, similar to the previous study with halo clustering (Nishimichi & Taruya 2011), allowing to incorporate the scale dependence of bias into the model, equation (8), through the following relation:

$$\delta_{\text{g}}(k) = b(k)\delta_{\text{m}}(k). \quad (14)$$

With this relation, the expression (8) is replaced with

$$P_{\text{g}}^s(k, \mu) = D_{\text{FoG}}(k\mu f\sigma_v) \times b(k)^2 \left[P_{\text{Kaiser}}(k, \mu; \beta) + b A(k, \mu; \beta) + b^2 B(k, \mu; \beta) \right], \quad (15)$$

where the quantity β is defined by $\beta = f/b$. For the function $b(k)$, we adopt the following parameterized form:

$$b(k) = b_0 \frac{1 + A_2 k^2}{1 + A_1 k}. \quad (16)$$

Note that the functional form (16) is quite close to the one introduced in Cole et al. (2005b).

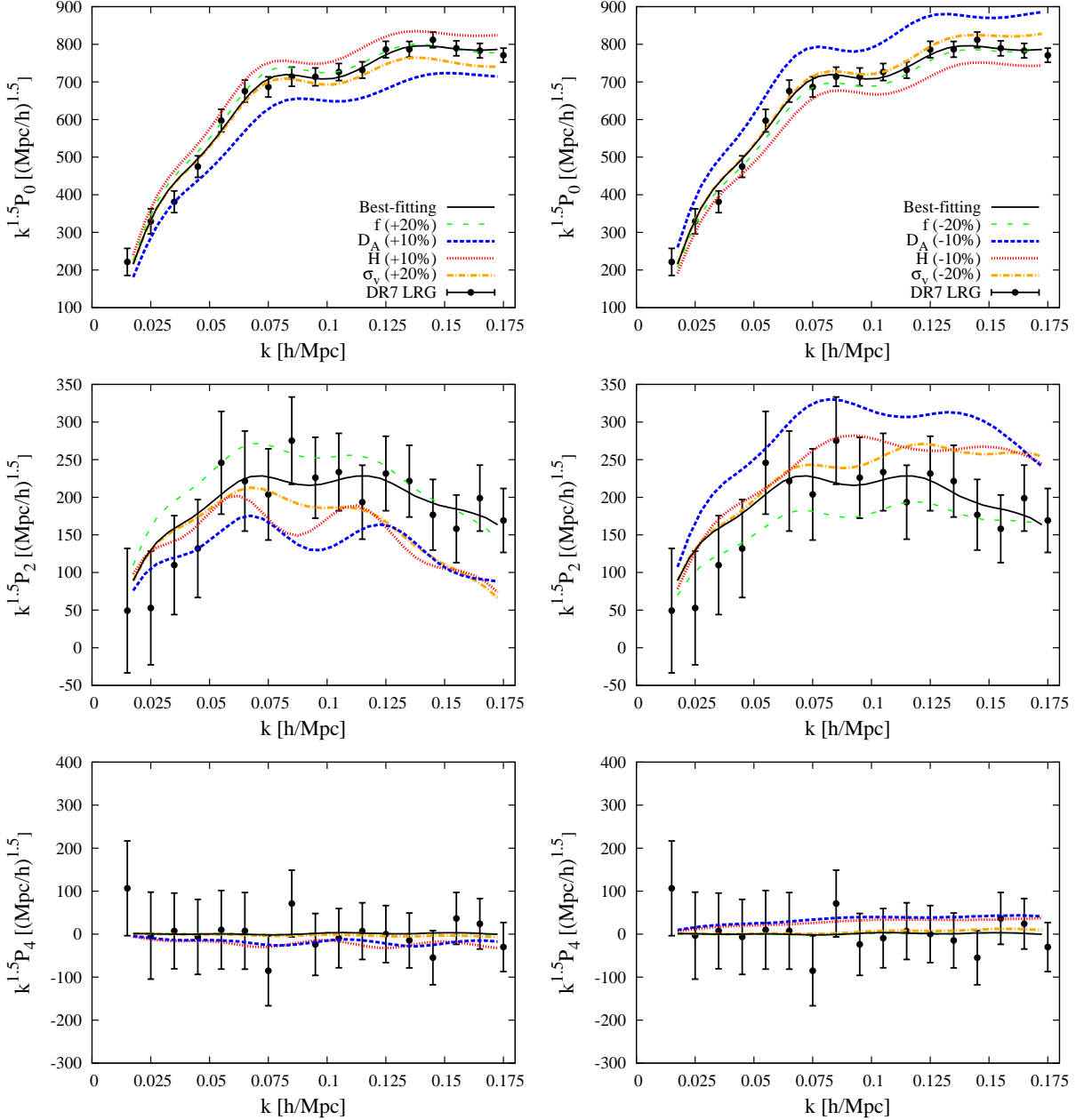


Figure 2. Variations of monopole (top), quadrupole (middle), and hexadecapole (bottom) power spectra computed with the PT model. We plot the best-fitting model of the SDSS DR7 LRG sample in solid curves (see Section 5 and Table. 1), but the other curves are the models with slightly shifting (left: increasing, right: decreasing) parameters, which characterize the linear Kaiser, FoG, and AP effects: f ($\pm 20\%$: (green; colors are available for the online version) dashed), D_A ($\pm 10\%$: (blue) dotted), H ($\pm 10\%$: (red) short-dotted), and σ_v ($\pm 20\%$: (orange) dot-dashed). For reference, the measured power spectra are also plotted by filled circles with error bars.

The scale-dependent linear bias has also been used to describe the redshift-space halo clustering. Adopting the parameterized function similar to equation (16), the model (8) successfully describes the multipole power spectra of haloes (Nishimichi & Taruya 2011). In this respect, albeit a rather phenomenological treatment, the model of equation (8) with equation (14) provides a practically useful prescription, and it is worth further testing the robustness with the mock subhalo catalogue described in the next section.

3.3 Alcock-Paczynski effect

Finally, the remaining effect to be incorporated into the theoretical template is the Alcock-Paczynski effect. The AP effect arises from the apparent mismatch of the underlying cosmology when we convert the redshift and angular position of each galaxy to the comoving radial and transverse distances, and it modulates the shape and amplitude of the multipole power spectra. Using the BAO scale as a standard ruler, this geometrical effect offers an attractive method to

measure the angular diameter distance $D_A(z)$ and Hubble parameter $H(z)$ of distance galaxies at redshift z .

The anisotropies caused by the AP effect can be modeled into the anisotropic power spectrum as

$$P^{\text{model}}(k, \mu) = \frac{H}{H^{\text{fid}}} \left(\frac{D_A^{\text{fid}}}{D_A} \right)^2 P_g^s(q, \nu). \quad (17)$$

Here, the comoving wavenumber k and the directional cosine μ measured with the underlying cosmological model are related to the true ones, q and ν , defined by

$$q(k, \mu) \equiv \alpha(\mu)k, \quad (18)$$

$$\nu(k, \mu) \equiv \frac{1}{\alpha(\mu)} \frac{H}{H^{\text{fid}}} \mu, \quad (19)$$

where the function $\alpha(\mu)$ is defined as

$$\alpha(\mu) \equiv \sqrt{\left(\frac{D_A^{\text{fid}}}{D_A} \right)^2 + \left[\left(\frac{H}{H^{\text{fid}}} \right)^2 - \left(\frac{D_A^{\text{fid}}}{D_A} \right)^2 \right] \mu^2}. \quad (20)$$

The quantities D_A^{fid} and H^{fid} are the fiducial values of the angular diameter distance and the Hubble parameter at a given redshift slice. Summing up all the ingredients, we model the multipole power spectra of the DR7 LRG as

$$P_\ell^{\text{model}}(k) = \frac{2\ell + 1}{2} \int_{-1}^1 d\mu \mathcal{L}_\ell(\mu) P^{\text{model}}(k, \mu). \quad (21)$$

In Fig. 2, we plot the multipole power spectra computed with our model, and show how the ingredients incorporated into our model change the shape and amplitude of the monopole (top), quadrupole (middle), and hexadecapole spectra (bottom). Here the solid curve is the best-fitting model of the DR7 LRG sample obtained in Section 5 (see Table.1), and the other curves are the models shifting the each parameter f , D_A , H , and σ_v by $\pm 10\%$ (see figure legend), while fixing others as well as the bias parameters ($b_0 = 2.03$, $A_1 = -0.615$, and $A_2 = 0.0392$). A slight increase in the linear growth rate f basically alters the quadrupole-to-monopole ratio through the linear Kaiser effect, and the FoG effect characterized by σ_v leads to a suppression of the amplitude of the spectra, especially in the quadrupole at the scale of our interest. On the other hand, the geometric quantities D_A and H change not only the acoustic scales in the monopole but also the shape and amplitude of the higher multipole spectra through the AP effect. Notably, the AP effect changes the quadrupole spectrum significantly. These characteristic behaviors indeed play an important role in the cosmological parameter estimation, and are the keys to robustly get simultaneous constraints on f , D_A , and H .

4 TESTING PT MODELS AGAINST MOCK CATALOGUES

In this section, we extensively examine the robustness of our model described in the previous section, and investigate in detail the applicable range of wavenumbers and the limitation of the model in order to correctly estimate the parameters f , D_A , and H . A great emphasis here is that we test the PT model against ‘realistic’ mock catalogues constructed with subhaloes identified from N -body simulations. There are several popular methods in the literature to construct mock catalogues, and these have been applied

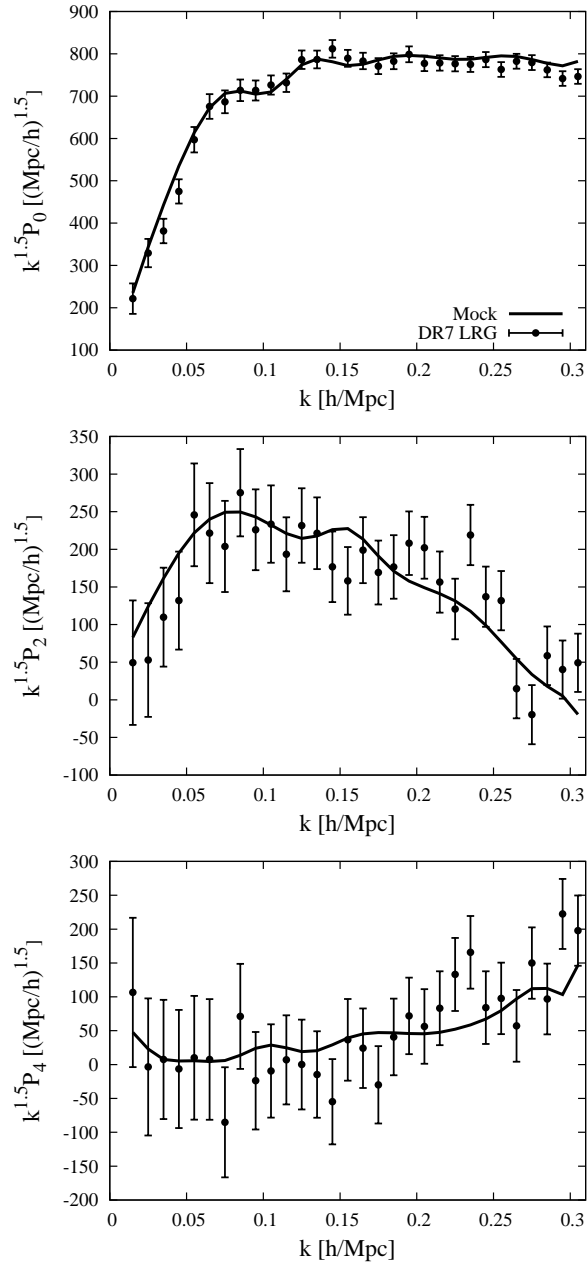


Figure 3. Monopole (top), quadrupole (middle), and hexadecapole (bottom) power spectra measured from our best-fitting mock catalogue and those of the SDSS DR7 LRG sample. The black solid lines correspond to our mock subhalo catalogue. The filled circles with error bars correspond to the SDSS DR7 LRG sample.

to characterize the observed properties of LRGs. The methods include the HOD modeling (Brown et al. 2008; Kulkarni et al. 2007; Reid et al. 2009b; Reid & Spergel 2009; White et al. 2007), and the subhalo abundance matching (SHAM) scheme (Conroy et al. 2006; Masaki et al. 2012). These mock subhalo catalogues are constructed such that they reproduce the observed number density, multiplicity function that determines the number distribution of LRGs hosted by the same halo, or the (angular) clustering on relatively small scales. In contrast, we construct mock catalogues on the

basis of the anisotropic clustering pattern of LRGs. To be more specific, we vary the threshold mass of haloes above which they can host LRGs (M_{\min}^{host}), the minimum mass of subhaloes for LRG candidates (M_{\min}^{sub}), and the fraction of satellite LRGs (R_S) and search for the parameters that best reproduce the observed multipole power spectra using the Markov-Chain Monte-Carlo (MCMC) method. This method is suitable for our purpose because the anisotropic clustering pattern is in general sensitive to the location and motion of galaxies, and these are thought to be tightly related to their size or mass along with the merger history of (sub)haloes.

In particular, subhaloes can exhibit a strong FoG effect in the measured multipole spectra due to the virial motion of satellites, i.e., less massive subhaloes away from the centre of each halo. We briefly explain how to generate our mock catalogues and refer to the accompanying paper (Nishimichi & Oka 2013) for more details on the mock construction.

In the latter part of this section, using these catalogues whose input cosmological parameters are a priori known by definition, we systematically examine our procedure to estimate the cosmological parameters of interest. Our mock test shows a successful performance, and hence validates our theoretical template and methodology which will be applied to the real data in the following section.

4.1 Generation of mock catalogues

We begin by describing the cosmological N -body simulations used in our analyses. We use 11 independent random realizations of cosmological N -body simulations presented in (Nishimichi & Taruya 2011), which are created by a publicly-available N -body code, `Gadget2` (Springel 2005). Each realization includes $N = 1,280^3$ dark matter particles in a cubic box with a side length of $1,144.72$ [Mpc/ h], which result in a particle mass of $5.54 \times 10^{10} [M_{\odot}/h]$. They assume a flat Λ CDM model with the cosmological parameters consistent with the five-year WMAP results (Komatsu et al. 2009); $\Omega_m = 0.279$, $\Omega_b = 0.046$, $h = 0.701$, $n_s = 0.96$ and $\sigma_8 = 0.817$. The initial conditions are generated at $z_{\text{in}} = 99$ using an initial condition generator developed in (Nishimichi et al. 2009; Valageas & Nishimichi 2011) based on the second-order Lagrangian perturbation theory (Crocco et al. 2006; Scoccimarro 1998b). Haloes and subhaloes are respectively identified with `Friends-of-Friends` (FoF; e.g. Davis et al. (1985)) and `SUBFIND` (Springel et al. 2001) algorithm from the dark matter positions and velocities at $z_{\text{out}} = 0.35$. In each halo, we distinguish the most massive subhalo from the rest, and conventionally call the most massive one *central*, while other remaining subhaloes are called *satellites*. Collecting the subhaloes that satisfy the criteria set by the three parameters (i.e., minimum mass of host haloes M_{\min}^{host} , minimum mass of subhaloes M_{\min}^{sub} and the fraction of satellite subhaloes R_S), we record their centre-of-mass positions and velocities to form mock LRGs (this catalogue is called as Model 4a in Nishimichi & Oka (2013)).

Provided the mock LRGs, the multipole moments of their power spectrum are measured as follows. We first evaluate the density field of subhaloes assigned on $1,024^3$ regular grid points by Nearest-Grid-Point interpolation technique (NGP). We then transform it into the Fourier space, and correct the window function by dividing by the NGP window kernel. Finally, with an appropriate weight depending on the

directional cosine of the wavevector (i.e., the Legendre polynomial, $\mathcal{L}_{\ell}(\mu)$), the density squared is fitted with the cubic B-spline function as function of wavenumber, from which the multipole spectra are evaluated at the wavenumbers where the observed power spectra are given. This method has an advantage over the standard power spectrum estimation with binned wavenumbers in the sense that the effect of finite number of grids over μ , which significantly affects the estimation of higher multipole spectra, is greatly reduced with cubic B-spline function. Note that the effect of finite grid size cannot be simply mitigated by increasing the number of simulations unless one changes the box size.

These above steps (i.e., construction of subhalo catalogues and estimation of the power spectrum) are repeated with different set of parameters, (M_{\min}^{host} , M_{\min}^{sub} , R_S). We compare the resultant power spectra with the observation to find the best-fitting mock catalogue to the DR7 LRGs. We carried out this with the MCMC algorithm. The properties of the best-fitting catalogue are discussed in the next subsection.

4.2 Properties of a best-fitting mock LRG catalogue

We use the best-fitting catalogue obtained in the accompanying paper (Nishimichi & Oka 2013). The best-fitting parameters for this catalogue are $M_{\min}^{\text{host}} = 9.81 \times 10^{12} M_{\odot}/h$, $M_{\min}^{\text{sub}} = 8.86 \times 10^{12} M_{\odot}/h$, $R_S = 0.26$ with $\chi^2/\text{d.o.f.} = 0.87$, where $\text{d.o.f.} = 30 \times 3 - 3 = 87$ is the total number of data points of $P_0(k_i)$, $P_2(k_i)$ and $P_4(k_i)$ in the range of the wavenumbers $k_i < k_{\text{max}} = 0.305$ [h/Mpc] (30 points for each) minus the number of free parameters (3). The multipole power spectra of this catalogue are shown in solid lines in Fig. 3. Overall, the power spectra measured from our mock catalogue reproduce the three observed moments, and the value of χ^2 indeed suggests that our mock is statistically consistent with the observation.

The satellite fraction of 26 %, which is significantly larger than that suggested from the Count-in-Cylinder (CiC) analysis (5 %; Reid & Spergel (2009)), mainly comes from the strong damping of the observed quadrupole moment towards high- k while successfully reproducing the amplitude of the monopole moment at the same time. These two results seem contradictory each other, but they would be understood as follows. The higher satellite fraction we found originates from the kinematical feature in RSDs, while the CiC analysis identified close galaxy pairs such that they both sit in the same massive halo. In other words, roughly 20% of satellite in our terminology could just correspond to a single LRG system in which the central galaxy is not observed or it has a significant off-centring (see Nishimichi & Oka (2013) in detail.)

The importance of the satellite fraction is also reported by Hikage & Yamamoto (2013), in which the authors discuss its effect on the higher multipole spectra of LRGs in redshift space. Since satellite galaxies have a velocity structure different from that of centrals, one can alter the multipole spectra, especially higher multipoles, by changing their fraction even when the HOD is kept unchanged. A larger satellite fraction means a larger velocity dispersion, and it leads to a stronger FoG damping required to explain the observed quadrupole.

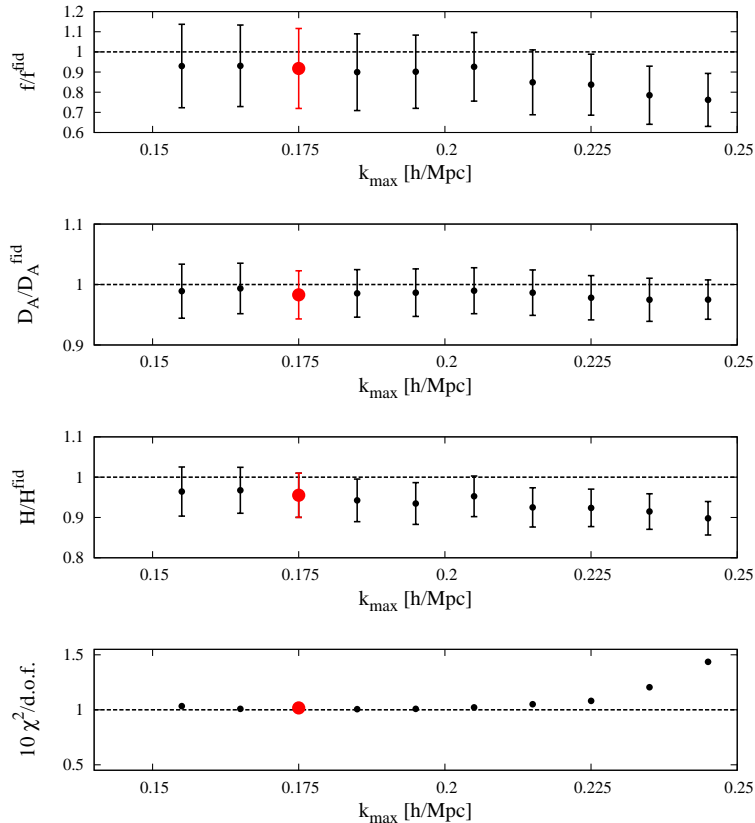


Figure 4. Performance of our fiducial model against the mock catalogues. We plot the best-fitting parameters for **WMAP5-z035** as a function of k_{\max} . The horizontal dotted lines show the fiducial values of the parameters. As is clear from this figure, the best-fitting parameters are consistent with the fiducial ones within $1\text{-}\sigma$ error up to $k_{\max} = 0.175[h/\text{Mpc}]$, which is marked as the large (red; colors are available for the online version) circle. For $k_{\max} > 0.175[h/\text{Mpc}]$, the perturbative approach breaks down because of the non-linearity. We plot $10\chi^2/\text{d.o.f.}$ in the bottom panel because we adopt the error on the power spectrum estimated for the SDSS DR7 LRG sample while the analysed mock spectra are measured from the total volume 11 times larger than the observation.

4.3 Test of systematics with the mock catalogue

In what follows, using the analytical model in Section 3, we analyse the multipole power spectra measured from the best-fitting mock LRG catalogue, and examine how well we can correctly recover the input cosmological parameters of the N -body simulations.

4.3.1 Method

We perform the MCMC analysis and try to fit the mock power spectrum with our analytical model under different assumptions. We investigate the sensitivity of the results to the maximum wavenumber (k_{\max}) included in the analyses, prior cosmological assumptions and the effective redshift of the galaxy sample, different theoretical models for RSDs and galaxy bias. We examine six different setups labeled as follows:

- **WMAP5-z035:** We here employ the full PT model, i.e., TNS model for RSDs with the linear scale-dependent galaxy bias given in equations (15) and (16), taking a proper account of the AP effect [equations(17)-(20)]. In computing the model power spectra, we adopt the same cosmological parameters as those used in the N -body simulations except

for D_A , H and f , and evaluate the spectra at $z = 0.35$, corresponding to the output redshift of the simulations.

- **WMAP5-P0P2:** Same as **WMAP5-z035**, but in fitting the model to the mock catalogue, we use only P_0 and P_2 .
- **WMAP5-z03:** Same as **WMAP5-z035**, but the model power spectra are evaluated at $z = 0.3$, slightly different from the output redshift $z = 0.35$.

It is indeed nontrivial to know an effective redshift of the DR7 LRG sample, and there is also an ambiguity in the effective redshift. Further, an evolution effect of LRGs over a wide redshift range, known as the light-cone effect (Yamamoto & Suto 1999), might lead to a misinterpretation of the cosmological results. We thus check if theoretical template at a slightly different redshift can correctly recover the cosmological parameters.

- **Planck:** Same as **WMAP5-z035**, but in computing the model power spectra, we adopt the cosmological parameters suggested by the Planck observation (Planck Collaboration 2013); $\Omega_m = 0.32$, $\Omega_b = 0.0496$, $h = 0.67$, $n_s = 0.96$, $\sigma_8 = 0.809$.

- **WMAP5-noAB:** Same as **WMAP5-z035**, but in computing the model power spectra, the A and B terms in the TNS model (8) are dropped out. A comparison with **WMAP5-z035** will show how much details of the model-

ing of RSD can affect the result of cosmological parameter estimations.

- **WMAP5-cbias**: Same as **WMAP5-z035**, but the galaxy bias model (14) is replaced with a constant bias, i.e. $b(k) = b_0$.

The setup of the MCMC analysis is summarized as follows. The total number of free parameters in our MCMC analysis is 7; the linear growth rate (f), the angular diameter distance (D_A), the Hubble parameter (H), the one-dimensional velocity dispersion in equation (8) (σ_v), and the bias parameters in equation (14) (b_0, A_1, A_2), except for **WMAP5-cbias**.

We find the best-fitting parameter set in the seven-dimensional parameter space by minimizing the chi-squared defined by

$$\chi^2 = \sum_{\ell=0,2,4} \sum_{i=1}^{N_{\text{bin}}} \left[\frac{P_{\ell}^{\text{model}}(k_i) - P_{\ell}^{\text{obs}}(k_i)}{\Delta P_{\ell}^{\text{obs}}(k_i)} \right]^2, \quad (22)$$

where $P_{\ell}^{\text{model}}(k_i)$ is defined by equation (21) and $P_{\ell}^{\text{obs}}(k_i)$ is the measured multipole power spectra. Note that $\ell = 4$ is not included in the case of **WMAP5-P0P2**. The error, $\Delta P_{\ell}^{\text{obs}}(k_i)$, is given by equation (7). Since we want to figure out the significance of possible systematics relative to the real observational errors, we will adopt the statistical error of the DR7 LRG to estimate $\Delta P_{\ell}^{\text{obs}}(k_i)$. In equation (22), the quantity N_{bin} denotes the number of k -bins, which depends on the maximum wavenumber k_{max} used for the parameter estimation. Below, we demonstrate how the MCMC results depends on k_{max} , and determine the appropriate value in our analysis. In the MCMC analysis, we use a part of publicly-available MCMC code *CosmoMC* (Lewis & Bridle 2002).

4.3.2 Results

In order to determine the applicable range of our theoretical template, we first examine the **WMAP5-z035** case, and perform the MCMC analysis varying the maximum wavenumber k_{max} from 0.155 to 0.245 [h/Mpc]. Figure 4 shows the goodness of fitting (i.e. $10\chi^2/\text{d.o.f.}$) and the marginalized 1- σ confidence intervals of the 3 parameters, f , D_A , and H as a function of k_{max} . As is seen from this figure, the best-fitting values correctly reproduce the fiducial value well within the 1- σ statistical confidence for $k_{\text{max}} \leq 0.175$ [h/Mpc]. The results look quite reasonable in the sense that the TNS model is accurate at a few percent level for the matter power spectrum at $z = 0.35$ (Taruya et al. 2012f, 2013a). At $k > 0.175$ [h/Mpc], the model prediction is known to deviate from dark matter simulations. Even though the estimated values of the 3 parameters are barely within 1- σ statistical confidence at $k_{\text{max}} = 0.205$ [h/Mpc], the value of H/H_{fid} is not properly estimated at $k_{\text{max}} \geq 0.185$ [h/Mpc]. This behavior presumably comes from some flaw of our analytical model. Thus, we conservatively adopt $k_{\text{max}} = 0.175$ [h/Mpc] in the following MCMC analysis, which corresponds to the number of bins, $N_{\text{bin}} = 17$.

We notice that the estimated values of (f, D_A, H) are a bit systematically lower than the fiducial values at any k_{max} . Since the underestimation is regarded as a systematic error in our modeling, these will be taken into account in the final result (see Section 5) as a systematic error to

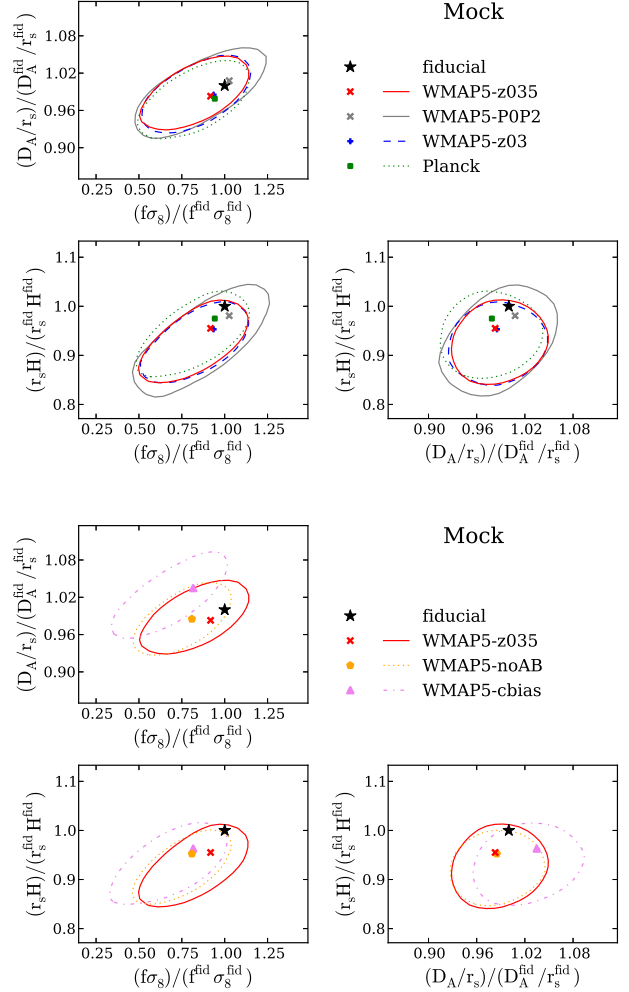


Figure 5. Test of systematics of our analysis using the mock catalogues for estimating the linear growth rate, angular diameter distance, and Hubble parameter. The star in each panel is the fiducial input parameters. We plot the best-fitting results with symbols and 68 % confidence contours for the different setup of the analysis (symbols and contours are plotted with the same color; available for the online version), **WMAP5-z035**, **WMAP5-P0P2**, **WMAP5-z03**, **Planck**, **WMAP5-noAB**, **WMAP5-cbias**, as noted in the figure. This figure shows that our model correctly recovers the fiducial cosmological model, and the incorrect cosmological assumptions are only marginal when taking the statistical error similar to the observed power spectra of LRGs in the SDSS DR7 into account. Note that in upper three panels, the distance scales D_A and H are also normalized by the sound horizon scales at baryon drag epoch, r_s , to highlight a difference in the measurement of distance scales themselves. Also, the linear growth rate is scaled by σ_8 . In lower three panels, the ratio $r_s/r_{s,\text{fid}}$ and $\sigma_8/\sigma_{8,\text{fid}}$ are unity because all the theoretical template is computed with the same underlying cosmology.

the total error budget. The systematic errors are evaluated as $(\pm 8.2\%, \pm 1.8\%, \pm 4.5\%)$ for (f, D_A, H) , respectively, at $k_{\text{max}} = 0.175$ [h/Mpc].

Let us now investigate possible systematics due to an incorrect cosmological prior or model assumptions. The results are summarized in Figs. 5 and 6. In Fig. 5, each pair

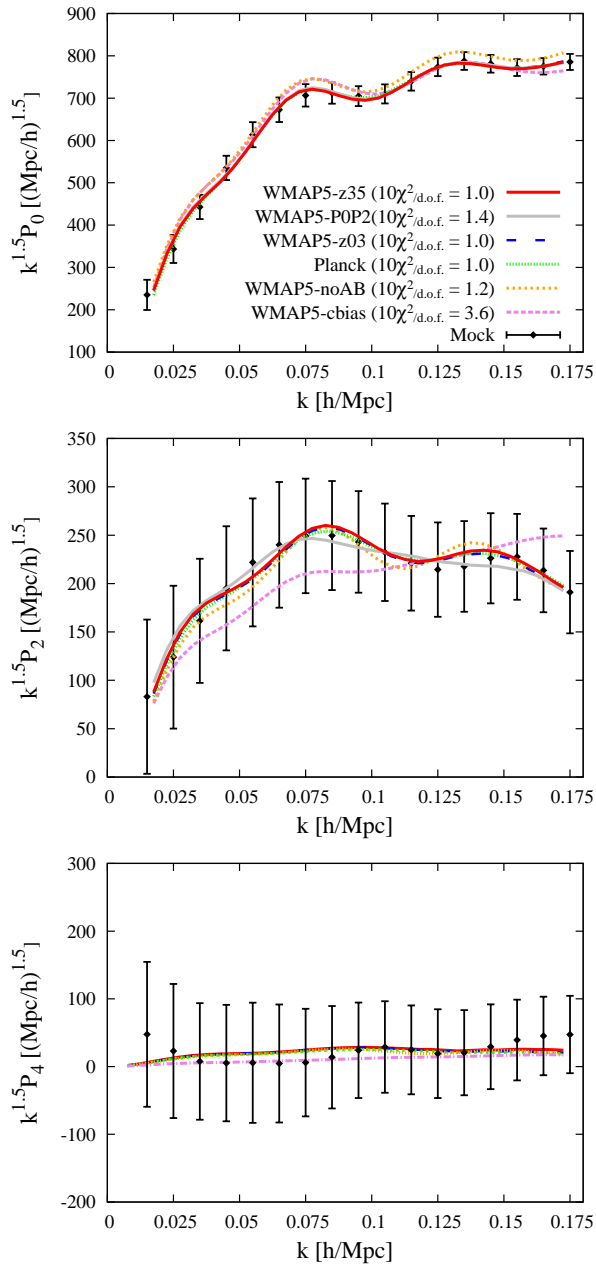


Figure 6. Comparisons of the multipole spectrum from the mock catalogues and the best-fitted curves for the different setups in Fig. 5. The meaning of the curves is noted in the top panel, the same as those of Fig. 5. The diamond shows the multipole power spectra measured from our mock catalogue. Note that the error bars show the statistical error for the SDSS DR7 LRG sample, and do not reflect the uncertainties of the mock power spectrum.

of the symbol and curve (with the same color; available for the online version) shows the best-fitting value and the 68% confidence contour from our fitting with the different setups, **WMAP5-z035** (solid red curve), **WMAP5-POP2** (solid gray curve), **WMAP5-z03** (dashed blue curve), **Planck** (dotted green curve), **WMAP5-noAB** (short-dotted orange curve), **WMAP5-cbias** (dot-dashed pink curve). The star in each panel is the fiducial input parameters. The upper three panels in Fig. 5 show that the input parameters

are recovered even if the prior assumption is slightly incorrect. The results of **WMAP5-z035** and **WMAP5-z03** are almost identical, which means that a choice of the effective redshift is not important. The contour of **WMAP5-z035** agrees with **Planck**, which means that the difference of cosmological parameters between **WMAP5-z035** and **Planck** does not systematically bias the results.

In these panels, we plot the combination $(f\sigma_8)/(f^{\text{fid}}\sigma_8^{\text{fid}})$, $[(D_A/r_s)/(D_A^{\text{fid}}/r_s^{\text{fid}})]$, and $(Hr_s)/(H^{\text{fid}}r_s^{\text{fid}})$ where r_s is the sound horizon scale at the baryon drag epoch. Thus, Fig. 5 highlights a difference in the measurements of the linear growth rate and distance scales themselves.

Here the sound horizon scale r_s is numerically evaluated with CAMB (Lewis et al. 2000). Also, by comparing **WMAP5-POP2** with **WMAP5-z035**, one sees that the hexadecapole improves the constraint marginally, which is qualitatively consistent with the Fisher matrix analysis (Taruya et al. 2011e). In lower three panels in Fig. 5, we demonstrate that our modeling of RSDs and galaxy bias successfully works in the sense that the best-fitting values of **WMAP5-z035** are closest to the fiducial input values compared to the other cases, **WMAP5-noAB** and **WMAP5-cbias**. However, the $1\text{-}\sigma$ contours of **WMAP5-noAB** and **WMAP5-cbias** contain the input parameters. These two setups, **WMAP5-noAB** and **WMAP5-cbias**, are also worse than **WMAP5-z035** in terms of the goodness of fitting. The value of $10\chi^2/\text{d.o.f.}$ for **WMAP5-noAB** and **WMAP5-cbias** is respectively 1.2 and 3.6 (see the legends in Fig. 6). We compare the best-fitting curves of the different setups in Fig. 6.

The authors of Taruya et al. (2010d); Nishimichi & Taruya (2011); Ishikawa et al. (2013) adopted a similar modeling of RSDs and galaxy bias, and showed a successful performance for the distribution of dark matter or haloes in the N -body simulations. Our results show that our modeling works for the galaxy mock catalogue as well.

5 COSMOLOGICAL ANALYSIS WITH THE SDSS DR7 LRG CATALOGUE

Let us now consider a simultaneous constraint on the cosmological parameters from the multipole power spectra of the DR7 LRGs, applying the method examined in the previous section. We compute the model power spectra, assuming a flat Λ CDM model with $(\Omega_m, \Omega_b, h, n_s, \sigma_8) = (0.32, 0.0496, 0.67, 0.96, 0.809)$ favored by the Planck result (Planck Collaboration 2013). Note that we assume the same redshift-distance relation as that in measuring the multipole power spectra from the DR7 LRG catalogue.

In the analysis of this section, we use the multipole power spectra of the DR7 LRGs up to $\ell = 4$ within the range of the wavenumber $k \leq k_{\text{max}} = 0.175$ [h/Mpc] (see Section 2), which includes $N_{\text{bin}} = 17$ equally-spaced bins for each multipole, unless explicitly stated otherwise.

5.1 Simultaneous constraints on f , D_A , and H

Our best-fitting model is shown together with the DR7

Setup	Redshift	$\chi^2/\text{d.o.f.}$	$f(z)$	$D_A(z)$ [Mpc]	$H(z)$ [km/s/Mpc]
Planck-z03 (canonical)	0.3	0.45	$0.71 \pm_{\text{stat.}} 0.12 \pm_{\text{sys.}} 0.06$	$968 \pm_{\text{stat.}} 42 \pm_{\text{sys.}} 17$	$81.7 \pm_{\text{stat.}} 5.0 \pm_{\text{stat.}} 3.7$
Planck-z035	0.35	0.50	$0.70 \pm_{\text{stat.}} 0.13 \pm_{\text{sys.}} 0.06$	$961 \pm_{\text{stat.}} 40 \pm_{\text{stat.}} 0.17$	$78.8 \pm_{\text{stat.}} 4.4 \pm_{\text{sys.}} 3.5$
WMAP5	0.3	0.46	$0.71 \pm_{\text{stat.}} 0.13 \pm_{\text{sys.}} 0.06$	$1012 \pm_{\text{stat.}} 41 \pm_{\text{sys.}} 18$	$78.3 \pm_{\text{stat.}} 4.4 \pm_{\text{sys.}} 3.5$
Planck-noAB	0.3	0.48	$0.65 \pm_{\text{stat.}} 0.12 \pm_{\text{sys.}} 0.05$	$967 \pm_{\text{stat.}} 39 \pm_{\text{sys.}} 17$	$80.7 \pm_{\text{stat.}} 3.9 \pm_{\text{sys.}} 3.6$
Planck-cbias	0.3	0.68	$0.68 \pm_{\text{stat.}} 0.13 \pm_{\text{sys.}} 0.06$	$1041 \pm_{\text{stat.}} 41 \pm_{\text{sys.}} 19$	$81.6 \pm_{\text{stat.}} 5.0 \pm_{\text{sys.}} 3.7$

Table 1. Test of systematics with the SDSS DR7 LRG sample, adopting the similar setups as those in Section 4.3. The best-fitting parameters and the goodness of fitting ($\chi^2/\text{d.o.f.}$) are listed. We adopt **Planck-z03** as a canonical setup, and the final results are obtained with this setup. The error denoted by *sys.* is the possible systematic error evaluated in the mock catalogue (see Section 4.3).

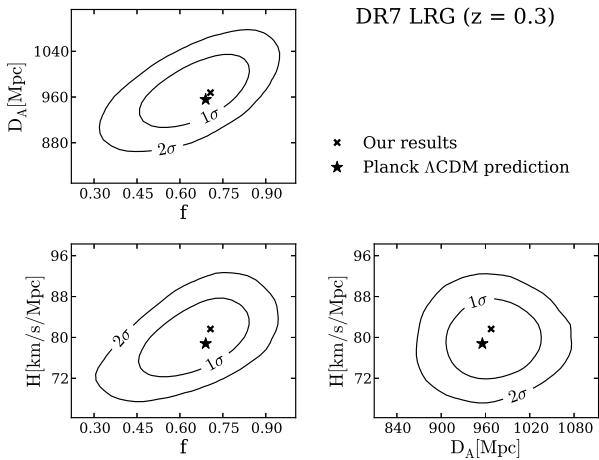


Figure 7. Simultaneous constraints on f , D_A , and H from the multipole power spectra of the SDSS DR7 LRG sample. In each panel, the inner and outer contours respectively represent 68 and 95 % confidence levels. We plot the best-fitting results in cross symbols as well as the ΛCDM prediction with the Planck cosmological parameters in stars.

LRG $P_\ell(k)$ in Fig. 1. Simultaneous constraints on f , D_A , and H marginalized over the other model parameters are presented in Fig. 7.

The value of $\chi^2/\text{d.o.f.}$ for our best-fitting model is 0.45, which is somewhat smaller than the expectation ($\chi^2/\text{d.o.f.} \sim 1$). The reason for the small $\chi^2/\text{d.o.f.}$ may partly come from the fact that we neglect the covariance both between different k s and ℓ s. We expect that full treatment of the covariance matrix can increase the χ^2 although we do not fully understand the reason why χ^2 is small. The estimated parameters, however, will not change significantly even when the off-diagonal components of covariance are taken into account as discussed in (Takahashi et al. 2009, 2011b).

In Fig. 7, we compare our results with the values predicted by the Planck best-fitting ΛCDM cosmology and find no evidence of significant discrepancy.

Let us discuss the degeneracy between (f, D_A, H) and the other nuisance parameters. The FoG parameter, σ_v , is strongly degenerated with the linear growth rate, f (the correlation coefficient $r(f, \sigma_v) = -0.62$). Also, the Hubble parameter, H , is moderately correlated with f and σ_v ($r(H, f) = 0.53$ and $r(H, \sigma_v) = -0.74$, respectively). These facts are not surprising since f , σ_v , and H are all sensitive to

the higher multipoles ($\ell = 2$ and 4), where a proper modeling of nonlinearity RSDs is essential. There is no significant degeneracy with the bias parameters, A_1 and A_2 , although the linear bias parameter, b_0 , has non-negligible correlations with D_A and H ($r(b_0, D_A) = 0.40$ and $r(b_0, H) = -0.75$, respectively).

Nonetheless, these degeneracies are not perfect. This fact implies that the power spectrum amplitude adds information on the geometric parameters, as opposed to the isotropic case. This is explained as follows. In principle, through the A-P effect, the power spectrum amplitude depends not only on b_0^2 but also on H/D_A^2 . But the degeneracy between these parameters cannot be broken without other extra information. With the measurement of BAO scale and RSD (roughly speaking, the quadrupole-to-monopole ratio, P_0/P_2), however, we can simultaneously estimate D_A^2/H and $f\sigma_8$, free from the bias parameters. Then, if we add the amplitude and shape information in the anisotropic power spectrum, which respectively depends on $b_0^2 H/D_A^2$ and $b_0^2 D_A H$, the degeneracy between b_0 , D_A and H is broken, and we can separately determine the geometric parameters (Padmanabhan & White 2008; Anderson et al. 2012; Percival et al. 2010b, 2007a).

We see that the correlations between the linear bias parameter, b_0 , and the geometric parameters, D_A and H are not perfect. This implies that the power spectrum amplitude may add information on the geometric parameters. As opposed to the isotropic case, this makes when the anisotropic part of the power spectrum is included in the following reason. The BAO scales and RSD (roughly speaking, the quadrupole-to-monopole ratio, P_0/P_2) respectively well constrain D_A^2/H and $f\sigma_8$ free from bias parameters. The degeneracy between D_A and H is broken by both amplitude and shape information in the anisotropic power spectrum, which respectively depends on $b_0^2 H/D_A^2$ and $b_0^2 D_A H$ (Padmanabhan & White 2008; Anderson et al. 2012; Percival et al. 2010b, 2007a).

Although we have already presented our main results, it would be still worthwhile mentioning how robust our modeling is against different setups as a check. Here we go through a similar study to what we have done for the mock catalogue. Namely, we compare constraints using several slightly different setups which are summarized in Table. 1. The labels of the setup in Table. 1 are summarized as follows.

- **Planck-z03:** The fiducial model described in the above. The redshift at which we evaluate the model power spectra is $z = 0.3$.
- **Planck-z035:** Same cosmological model as **Planck-**

z03 but we evaluate the model power spectra at $z = 0.35$, which is normally quoted as the effective redshift in the FKP-type measurement (Percival et al. 2010b).

- **WMAP5**: We assume the cosmological parameters favored by the WMAP 5-yr result, $\Omega_m = 0.28$, $\Omega_b = 0.046$, $h = 0.7$, $n_s = 0.96$, $\sigma_8 = 0.8$, and $z = 0.3$, for computing the model spectra.

- **Planck-noAB**: Same as **Planck-z03**, but with the A and B correction terms in the RSD model (8) dropped out.

- **Planck-cbias**: Same as **Planck-z03**, but with the galaxy bias (14) being a constant, i.e., $b(k) = b_0$.

As is seen from Table. 1, **Planck-z03** gives the smallest χ^2 , while the difference is small. The constraints on (f, D_A, H) are all consistent with each other, excepting **Planck-cbias**. The bias parameters are in fact more important than the others in order to well fit to the monopole. Comparison between **WMAP5** and **Planck-z03** shows that our constraints are not sensitive to choice of the underlying cosmology for the model power spectrum. We thus conclude that our results are robust against such systematics.

5.2 Comparison with previous works

Here let us mention the consistency of our results compared with previous works. We show some examples of similar works (Blake et al. 2011b; Reid et al. 2012a; Samushia et al. 2012; Xu et al. 2013) in Fig. 8 and Table. 2, together with the predictions from different cosmological models. Fig. 8 shows that all of the results tend to underestimate $f\sigma_8$ compared to the Planck best-fitting Λ CDM model but no significant deviation from a Λ CDM model is confirmed. Our results are in a good agreement with those in Samushia et al. (2012); Xu et al. (2013), in which the same galaxy sample, i.e., the DR7 LRGs is used with different statistics or setups.

The solid and dotted lines respectively show theoretical prediction in a flat Λ CDM model with the Planck and WMAP-5yr cosmological parameters. We here also plot the linear growth rate of DGP model (Dvali et al. 2000) with Planck cosmological parameters, as one of the representative modified gravity models.

While we put such a simultaneous constraint using the multipole power spectra for the first time up to the hexadecapole moment, our results are consistent with previous works (Samushia et al. 2012; Xu et al. 2013). Samushia et al. (2012) measured the linear growth rate, f from the LRG sample, but they ignored the AP effect and used a different approach with the correlation function. On the other hand, Xu et al. (2013) investigated the AP effect through the location of the BAO ring, marginalizing over the broadband shape information. Also, note that Xu et al. (2013) adopted the reconstruction procedure of the BAO feature so that they can see the signal more clearly. Their measurement errors on D_A and H (3.6% for D_A and 8.4% for H) are somewhat similar to what we obtain (4.3% for D_A and 6.1% for H), even though we utilize the broadband shape information in the anisotropic power spectrum. These results suggest that the impact of the AP effect on the isotropic part (P_0) is mostly constrained through the shift of the location of the BAO signature, while the change of the overall amplitude and shape is somewhat absorbed in the bias

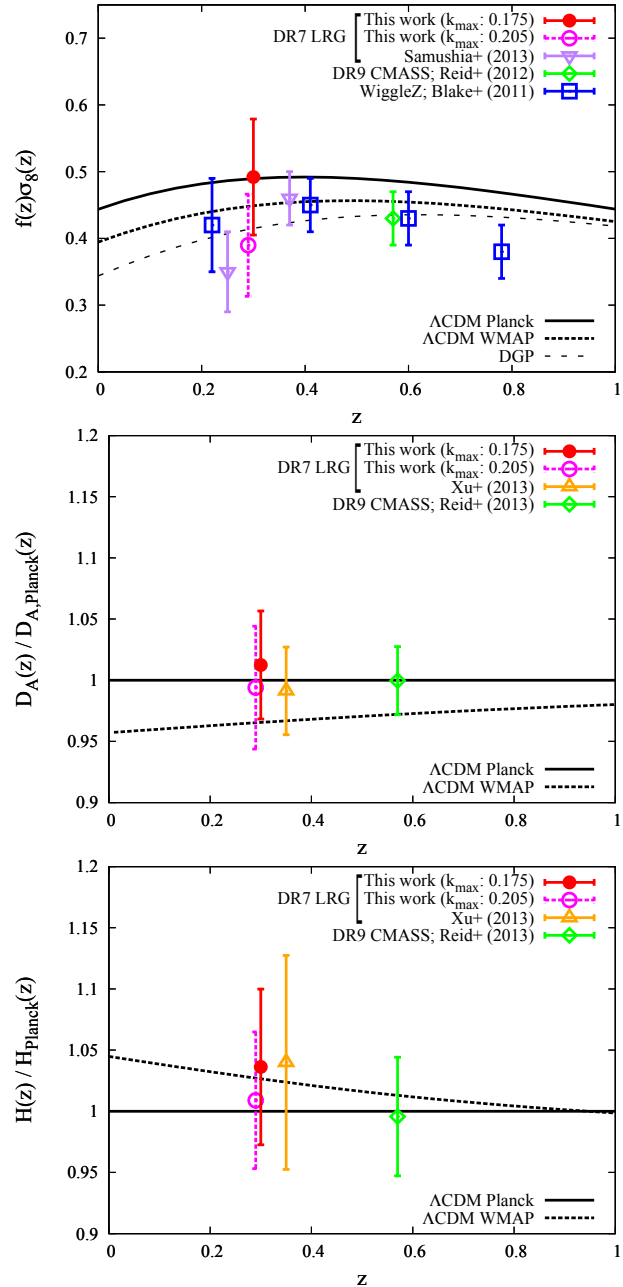


Figure 8. Comparisons of our results with those of previous works and model predictions. The linear growth rate (top), angular diameter distance (middle), and Hubble parameter (bottom) as a function of redshift are shown. We plot our results with $k_{max} = 0.175[h/\text{Mpc}]$ in filled (red); colors are available for the online version) circles as well as our aggressive results with $k_{max} = 0.205[h/\text{Mpc}]$ in open (magenta) circles to caveat the systematic due to non-linear RSDs. For comparison, we also display an open (purple) inverted triangle from (Samushia et al. 2012), open (blue) boxes from (Blake et al. 2011b), open (green) diamonds from (Reid et al. 2012a), and open (orange) triangles from (Xu et al. 2013). The solid curve is the prediction of the flat Λ CDM assumption with the Planck cosmological parameters ($\Omega_m = 0.32$, $h = 0.67$) (Planck Collaboration 2013) and the dotted curve is those of the WMAP cosmological parameters ($\Omega_m = 0.279$, $h = 0.701$) (Komatsu et al. 2009). On the other hand, the dashed curve is the prediction of the DGP model (Dvali et al. 2000). Note that we here do not include the systematic errors for our result.

function. On the other hand, the signature of BAOs on the anisotropic part (P_2 and P_4) is not clear given the current level of the statistical error. Instead, the broadband shape of these moments that can significantly be altered by the AP effect might give most of the information (Padmanabhan & White 2008), leading to the difference from the result in Xu et al. (2013).

Let us emphasize again that our study is the first attempt to constrain simultaneously on the gravitational growth and the cosmic distance scale especially with the multipole power spectra up to the hexadecapole ($\ell = 4$). Reid et al. (2012a) made a similar effort for the BOSS DR9 CMASS sample but they restrict the analysis to the monopole and quadrupole moments of the two-point correlation function. The two-point correlation function in principle carries the same cosmological information with the power spectrum but may suffer from somewhat different systematics issues (Reid & White 2011), and hence a consistency check between the two analyses would be important to validate the results.

5.3 What happens if aggressively fitted with higher k_{\max} ?

Even though we have already presented the main results of this study, it might still be interesting to see what happens if we aggressively adopted a higher k_{\max} . One may wish to obtain tighter constraints with adopting a higher k_{\max} . As we address in this paper, however, a smaller error does not necessarily assure a better constraint unless systematics both in the modeling and the measurements are well under control. In this subsection, we revisit a similar study to what we have done with the mock catalogues, and show how the results change as k_{\max} is varied.

Fig. 9 plots the one-dimensional constraints on f, D_A, H , and the goodness of fitting, as a function of k_{\max} . Interestingly, there is a notable tension ($\sim 20\%$) between the derived values of the linear growth rate f with $k_{\max} = 0.175$ and 0.205 [h/Mpc], while D_A and H are in good agreement (Fig. 7). We have not observed such a behavior in the mock analyses (see Fig. 4). In order to understand the cause of the discrepancy, we compare the best-fitting curves for each k_{\max} in Fig. 10. We argue that the discrepancy is driven by the fact that the measured quadrupole spectrum has data points somewhat larger than the line with $k_{\max} = 0.175$ [h/Mpc]. This kind of feature in the quadrupole spectrum is not confirmed in the mocks, and it is hard to tell what really causes the behavior. One reason could be the sample variance which is suppressed by a large number of realizations of the mock catalogues. The limitation of our model is likely to be another reason. We have some signs from an analysis of the velocity statistics in the simulations that our treatment of the FoG suppression with a constant σ_v does not fully capture the pairwise velocity statistics in the simulations (see e.g. Lam et al. (2011) for a recent study on the pairwise velocity). Also, the effect of the 1-halo term could start to be dominant around the scales (Valageas & Nishimichi 2011; Hikage & Yamamoto 2013).

6 SUMMARY AND DISCUSSIONS

In this paper, we quantitatively study the anisotropic clustering of the SDSS DR7 LRG sample in order to simultaneously constrain the growth of structure via the RSDs and the cosmic distance scales via the AP effects. Using the multipole power spectra up to the hexadecapole ($\ell = 4$), we obtain robust constraints on the linear growth rate $f(z = 0.3) = 0.71 \pm_{\text{stat.}} 0.12 \pm_{\text{sys.}} 0.06$, the angular diameter distance $D_A(z = 0.3) = 968 \pm_{\text{stat.}} 42 \pm_{\text{sys.}} 17$ [Mpc], and the Hubble parameter $H(z = 0.3) = 81.7 \pm_{\text{stat.}} 5.0 \pm_{\text{sys.}} 3.7$ [km/s/Mpc]. Note that this result is based on $\sigma_8(z = 0.3) = 0.696$.

A remarkable point in this study is that we test our modeling systematics against ‘realistic’ mock catalogues. Our mock catalogues consist of subhaloes identified in N -body simulations characterized by three parameters; the mass thresholds of host haloes (M_{\min}^{host}) and subhaloes (M_{\min}^{sub}), and satellite fraction R_S . With a suitable choice of the parameter set (see Section 4.2), the subhalo catalogue quantitatively explain the clustering properties of LRGs (Nishimichi & Oka 2013), and it consistently reproduces the measured multipole power spectra. Then, we model the anisotropic galaxy power spectrum on the basis of perturbation theory. Combining with a phenomenological treatment of the galaxy bias, the robustness of our theoretical template is extensively tested against the subhalo catalogue. At a relevant redshift of the SDSS DR7 LRG sample, our model power spectra used as the fitting template are found to be valid up to $k_{\max} = 0.175$ [h/Mpc], and can correctly recover the input values of the underlying cosmological model. Hence, applying the same analytical model to the real observations, robust cosmological constraints on f, D_A , and H have finally been obtained.

The derived cosmological constraints are fully consistent with a flat Λ CDM cosmology. The other cosmological results based on the anisotropic galaxy clustering are also consistent with a flat Λ CDM cosmology which implicitly assumes general relativity as the underlying theory of gravity. Although the measured values of the linear growth rate tend to slightly deviate from the Planck best-fitting Λ CDM model, more refined galaxy samples are definitely needed to statistically pin down the possible reasons of this. The galaxy samples with larger volumes, including the BOSS CMASS and LOWZ, continue to improve the measurement errors, and hence can be also used as more stringent tests of general relativity. With a sophisticated template taking account of the modification of gravity, we can further address the test of gravity beyond a consistency test, and put a tight constraint on theories of modified gravity (Taruya et al. 2013b).

As we have seen in Fig. 10 (see Section 5.3), an aggressive analysis of the power spectrum data up to a higher k_{\max} results in a 20% difference in the measurement of the linear growth rate. While this fact may be partly explained by the sample variance, it also implies that we do need a more elaborate modeling of non-linear RSDs if we want to push to smaller scales where higher signal-to-noise ratios are expected (see Hikage & Yamamoto (2013) along this line). As increasing the statistical power, a more careful analysis combining the perturbation theory or a new theoretical framework with the simulations will be definitely important for robust cosmological constraints. We believe that the present

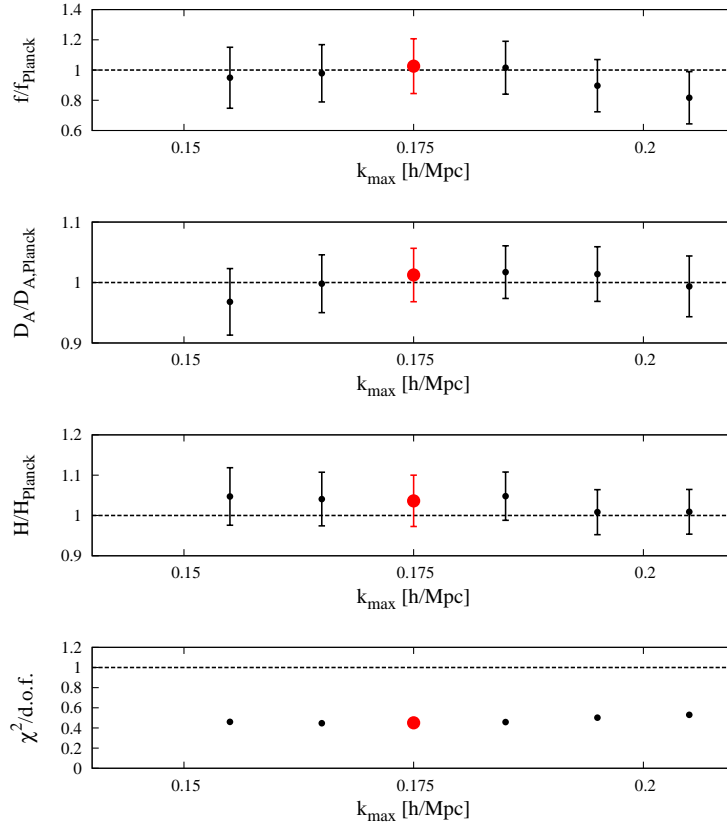


Figure 9. Similar figures to Fig. 4 but with the SDSS DR7 LRG sample. We plot the best-fitting parameters for **Planck-z03** as a function of k_{\max} . The horizontal dotted lines show the Λ CDM prediction with the Planck cosmological parameters. The large (red; available for the online version) circle is our canonical results with $k_{\max} = 0.175[h/\text{Mpc}]$. A remarkable difference ($\sim 20\%$) between the canonical results and the aggressive results with $k_{\max} = 0.205[h/\text{Mpc}]$ appears in estimated value of f , while such behavior was not seen in the analysis with the mock LRG catalogue (see Section 4.3).

approach with the subhalo catalogue provides a useful way to validate the RSD modeling, and can be generally applied to any galaxy redshift surveys. We hope to report such an analysis elsewhere.

ACKNOWLEDGEMENTS

Authors thank Yasushi Suto for fruitful comments to the systematic study. Authors also thank Jun’ichi Yokoyama, Naoki Yoshida, Masahiro Takada, Takahiko Matsubara, Shirley Ho, and Chiaki Hikage for useful discussion. AO acknowledges technical support from Toshiya Kashiwagi. This work is supported in part by a Grant-in-Aid from the Japan Society for the Promotion of Science (JSPS) (No. 24540257 for AT and No. 25887012 for SS). TN is supported by JSPS Postdoctoral Fellowships for Research Abroad. The research by K.Y. is supported in part by Grant-in-Aid for Scientific researcher of Japanese Ministry of Education, Culture, Sports, Science and Technology (No. 21540270 and No. 21244033).

REFERENCES

Abazajian K. N. et al., 2009, *ApJ Suppl.*, 182, 543,

[arXiv:0812.0649](https://arxiv.org/abs/0812.0649)

Ahn C. P. et al., 2013, preprint, [arXiv:1307.7735](https://arxiv.org/abs/1307.7735)

Alcock C., Paczynski B., 1979, *Nature*, 281, 358

Anderson L. et al., 2012, *MNRAS*, 427, 3435,

[arXiv:1203.6594](https://arxiv.org/abs/1203.6594)

Ballinger W. E., Peacock J. A., Heavens A. F., 1996, *MNRAS*, 282, 877, [arXiv:astro-ph/9605017](https://arxiv.org/abs/astro-ph/9605017)

Bernardeau F., Colombi S., Gaztañaga E., Scoccimarro R., 2002, *Physics Reports*, 367, 1, [arXiv:astro-ph/0112551](https://arxiv.org/abs/astro-ph/0112551)

Bertschinger E., 2006, *ApJ*, 648, 797, [arXiv:astro-ph/0604485](https://arxiv.org/abs/astro-ph/0604485)

Beutler F. et al., 2011, *MNRAS*, 416, 3017, [arXiv:1106.3366](https://arxiv.org/abs/1106.3366)

Blake C. et al., 2009a, preprint, [arXiv:0901.2587](https://arxiv.org/abs/0901.2587)

Blake C. et al., 2011b, *MNRAS*, 415, 2876, [arXiv:1104.2948](https://arxiv.org/abs/1104.2948)

Blake C. et al., 2011c, *MNRAS*, 418, 1707, [arXiv:1108.2635](https://arxiv.org/abs/1108.2635)

Brown M. J. I. et al., 2008, *ApJ*, 682, 937, [arXiv:0804.2293](https://arxiv.org/abs/0804.2293)

Chuang C.-H., Wang Y., 2012a, *MNRAS*, 426, 226, [arXiv:1102.2251](https://arxiv.org/abs/1102.2251)

Chuang C.-H., Wang Y., 2013b, *MNRAS*, 431, 2634, [arXiv:1205.5573](https://arxiv.org/abs/1205.5573)

Chuang C.-H., Wang Y., 2013c, *MNRAS*, 435, 255, [arXiv:1209.0210](https://arxiv.org/abs/1209.0210)

Cole S., Fisher K. B., Weinberg D. H., 1994a, *MNRAS*, 267, 785, [arXiv:astro-ph/9308003](https://arxiv.org/abs/astro-ph/9308003)

Cole S. et al., 2005b, *MNRAS*, 362, 505, [arXiv:astro-ph/0505001](https://arxiv.org/abs/astro-ph/0505001)

- ph/0501174
- Colless M. et al., 2001, MNRAS, 328, 1039, [arXiv:astro-ph/0106498](#)
- Conroy C., Wechsler R. H., Kravtsov A. V., 2006, ApJ, 647, 201, [arXiv:astro-ph/0512234](#)
- Contreras C. et al., 2013, MNRAS, 430, 924, [arXiv:1302.5178](#)
- Cooray A., Sheth R., 2002, Physics Reports, 372, 1, [arXiv:astro-ph/0206508](#)
- Crocce M., Pueblas S., Scoccimarro R., 2006, MNRAS, 373, 369, [arXiv:astro-ph/0606505](#)
- Davis M., Efstathiou G., Frenk C. S., White S. D. M., 1985, ApJ, 292, 371
- Dvali G., Gabadadze G., Porrati M., 2000, Physics Letters B, 485, 208, [arXiv:hep-th/0005016](#)
- Eisenstein D. J. et al., 2001a, AJ, 122, 2267, [arXiv:astro-ph/0108153](#)
- Eisenstein D. J. et al., 2005b, ApJ, 633, 560, [arXiv:astro-ph/0501171](#)
- Ellis R. et al., 2012, preprint, [arXiv:1206.0737](#)
- Feldman H. A., Kaiser N., Peacock J. A., 1994, ApJ, 426, 23, [arXiv:astro-ph/9304022](#)
- Guzzo L. et al., 2008, Nature, 451, 541, [arXiv:0802.1944](#)
- Hamilton A. J. S., 1995a, in Maurogordato S., Balkowski C., Tao C., Tran Thanh Van J., eds, Clustering in the Universe. p. 143, [arXiv:astro-ph/9507022](#)
- Hamilton A. J. S., 1998b, in Hamilton D., ed., Astrophysics and Space Science Library Vol. 231, The Evolving Universe. p. 185, [arXiv:astro-ph/9708102](#)
- Hatton S., Cole S., 1999, MNRAS, 310, 1137, [arXiv:astro-ph/9905186](#)
- Hemantha M. D. P., Wang Y., Chuang C.-H., 2013, ArXiv e-prints, [arXiv:1310.6468](#)
- Hikage C., Yamamoto K., 2013, JCAP, 8, 19, [arXiv:1303.3380](#)
- Hikage C., Mandelbaum R., Takada M., Spergel D. N., 2012a, ArXiv e-prints, [arXiv:1211.1009](#)
- Hikage C., Takada M., Spergel D. N., 2012b, MNRAS, 419, 3457, [arXiv:1106.1640](#)
- Hinshaw G. et al., 2012, preprint, [arXiv:1212.5226](#)
- Ishikawa T., Totani T., Nishimichi T., Takahashi R., Yoshida N., Tonegawa M., 2013, preprint, [arXiv:1308.6087](#)
- Jackson J. C., 1972, MNRAS, 156, 1P
- Jain B., Khoury J., 2010, Annals of Physics, 325, 1479, [arXiv:1004.3294](#)
- Kaiser N., 1987, MNRAS, 227, 1
- Kimura R., Kobayashi T., Yamamoto K., 2012, Phys. Rev. D, 85, 123503, [arXiv:1110.3598](#)
- Komatsu E. et al., 2009, ApJ Suppl., 180, 330, [arXiv:0803.0547](#)
- Kravtsov A. V., Berlind A. A., Wechsler R. H., Klypin A. A., Gottlöber S., Allgood B., Primack J. R., 2004, ApJ, 609, 35, [arXiv:astro-ph/0308519](#)
- Kulkarni G. V., Nichol R. C., Sheth R. K., Seo H.-J., Eisenstein D. J., Gray A., 2007, MNRAS, 378, 1196, [arXiv:astro-ph/0703340](#)
- Lam T. Y., Nishimichi T., Yoshida N., 2011, MNRAS, 414, 289, [arXiv:1008.0406](#)
- Laureijs R. et al., 2011, preprint, [arXiv:1110.3193](#)
- Levi M. et al., 2013, preprint, [arXiv:1308.0847](#)
- Lewis A., Bridle S., 2002, Phys. Rev. D, 66, 103511, [arXiv:astro-ph/0205436](#)
- Lewis A., Challinor A., Lasenby A., 2000, ApJ, 538, 473, [arXiv:astro-ph/9911177](#)
- Masaki S., Hikage C., Takada M., Spergel D. N., Sugiyama N., 2012, preprint, [arXiv:1211.7077](#)
- Matsubara T., 2013a, preprint, [arXiv:1304.4226](#)
- Matsubara T., 2008b, Phys. Rev. D, 77, 063530, [arXiv:0711.2521](#)
- Matsubara T., 2008c, Phys. Rev. D, 78, 083519, [arXiv:0807.1733](#)
- Matsubara T., 2011d, Phys. Rev. D, 83, 083518, [arXiv:1102.4619](#)
- Matsubara T., 2004e, ApJ, 615, 573, [arXiv:astro-ph/0408349](#)
- Matsubara T., Suto Y., 1996, ApJL, 470, L1, [arXiv:astro-ph/9604142](#)
- Nishimichi T., Oka A., 2013, ArXiv e-prints, [arXiv:1310.2672](#)
- Nishimichi T., Taruya A., 2011, Phys. Rev. D, 84, 043526, [arXiv:1106.4562](#)
- Nishimichi T. et al., 2009, PASJ, 61, 321, [arXiv:0810.0813](#)
- Okumura T., Seljak U., McDonald P., Desjacques V., 2012a, JCAP, 2, 10, [arXiv:1109.1609](#)
- Okumura T., Seljak U., Desjacques V., 2012b, JCAP, 11, 14, [arXiv:1206.4070](#)
- Padmanabhan N., White M., 2008, Phys. Rev. D, 77, 123540, [arXiv:0804.0799](#)
- Peebles P. J. E., 1980, The large-scale structure of the universe
- Percival W. J., Cole S., Eisenstein D. J., Nichol R. C., Peacock J. A., Pope A. C., Szalay A. S., 2007a, MNRAS, 381, 1053, [arXiv:0705.3323](#)
- Percival W. J. et al., 2010b, MNRAS, 401, 2148, [arXiv:0907.1660](#)
- Perlmutter S. et al., 1999, ApJ, 517, 565, [arXiv:astro-ph/9812133](#)
- Planck Collaboration 2013, preprint, [arXiv:1303.5076](#)
- Reid B. A., Spergel D. N., 2009, ApJ, 698, 143, [arXiv:0809.4505](#)
- Reid B. A., White M., 2011, preprint, [arXiv:1105.4165](#)
- Reid B. A. et al., 2012a, MNRAS, 426, 2719, [arXiv:1203.6641](#)
- Reid B. A., Spergel D. N., Bode P., 2009b, ApJ, 702, 249, [arXiv:0811.1025](#)
- Riess A. G. et al., 1998, AJ, 116, 1009, [arXiv:astro-ph/9805201](#)
- Samushia L., Percival W. J., Raccanelli A., 2012, MNRAS, 420, 2102, [arXiv:1102.1014](#)
- Sargent W. L. W., Turner E. L., 1977, ApJL, 212, L3
- Sato T., Hütsi G., Nakamura G., Yamamoto K., 2013a, ArXiv e-prints, [arXiv:1308.3551](#)
- Sato T., Hütsi G., Yamamoto K., 2011b, Progress of Theoretical Physics, 125, 187, [arXiv:1010.0289](#)
- Scoccimarro R., 2004a, Phys. Rev. D, 70, 083007, [arXiv:astro-ph/0407214](#)
- Scoccimarro R., 1998b, MNRAS, 299, 1097, [arXiv:astro-ph/9711187](#)
- Seljak U., McDonald P., 2011, JCAP, 11, 39, [arXiv:1109.1888](#)
- Seo H.-J., Eisenstein D. J., 2003, ApJ, 598, 720, [arXiv:astro-ph/0307460](#)

Seo H.-J. et al., 2012, ApJ, 761, 13, [arXiv:1201.2172](#)
 Springel V., 2005, MNRAS, 364, 1105, [arXiv:astro-ph/0505010](#)
 Springel V., White S. D. M., Tormen G., Kauffmann G., 2001, MNRAS, 328, 726, [arXiv:astro-ph/0012055](#)
 Suzuki N. et al., 2012, ApJ, 746, 85, [arXiv:1105.3470](#)
 Takahashi R. et al., 2009, ApJ, 700, 479, [arXiv:0902.0371](#)
 Takahashi R. et al., 2011b, ApJ, 726, 7, [arXiv:0912.1381](#)
 Taruya A., Koyama K., Hiramatsu T., Oka A., 2013b, ArXiv e-prints, [arXiv:1309.6783](#)
 Taruya A., Nishimichi T., Bernardeau F., 2013a, preprint, [arXiv:1301.3624](#)
 Taruya A., Nishimichi T., Saito S., Hiramatsu T., 2009c, Phys. Rev. D, 80, 123503, [arXiv:0906.0507](#)
 Taruya A., Nishimichi T., Saito S., 2010d, Phys. Rev. D, 82, 063522, [arXiv:1006.0699](#)
 Taruya A., Saito S., Nishimichi T., 2011e, Phys. Rev. D, 83, 103527, [arXiv:1101.4723](#)
 Taruya A., Bernardeau F., Nishimichi T., Codis S., 2012f, Phys. Rev. D, 86, 103528, [arXiv:1208.1191](#)
 Valageas P., Nishimichi T., 2011, A&A, 527, A87, [arXiv:1009.0597](#)
 Vlah Z., Seljak U., Okumura T., Desjacques V., 2013a, ArXiv e-prints, [arXiv:1308.6294](#)
 Vlah Z., Seljak U., McDonald P., Okumura T., Baldauf T., 2012b, JCAP, 11, 9, [arXiv:1207.0839](#)
 Wang L., Reid B., White M., 2013, preprint, [arXiv:1306.1804](#)
 Weinberg D. H., Mortonson M. J., Eisenstein D. J., Hirata C., Riess A. G., Rozo E., 2013, Physics Reports, 530, 87, [arXiv:1201.2434](#)
 White M., Zheng Z., Brown M. J. I., Dey A., Jannuzi B. T., 2007, ApJL, 655, L69, [arXiv:astro-ph/0611901](#)
 Xu X., Cuesta A. J., Padmanabhan N., Eisenstein D. J., McBride C. K., 2013, MNRAS, 431, 2834, [arXiv:1206.6732](#)
 Yamamoto K., Suto Y., 1999, ApJ, 517, 1, [arXiv:astro-ph/9812486](#)
 Yamamoto K., Nakamichi M., Kamino A., Bassett B. A., Nishioka H., 2006a, PASJ, 58, 93, [arXiv:astro-ph/0505115](#)
 Yamamoto K., Nakamura G., Hütsi G., Narikawa T., Sato T., 2010b, Phys. Rev. D, 81, 103517, [arXiv:1004.3231](#)
 Yamamoto K., Sato T., Hütsi G., 2008c, Progress of Theoretical Physics, 120, 609, [arXiv:0805.4789](#)
 Yoo J., Seljak U., 2013, preprint, [arXiv:1308.1093v1](#)
 Zheng Z., Zehavi I., Eisenstein D. J., Weinberg D. H., Jing Y., 2008, ApJ, 707, 554, [arXiv:0809.1868](#)

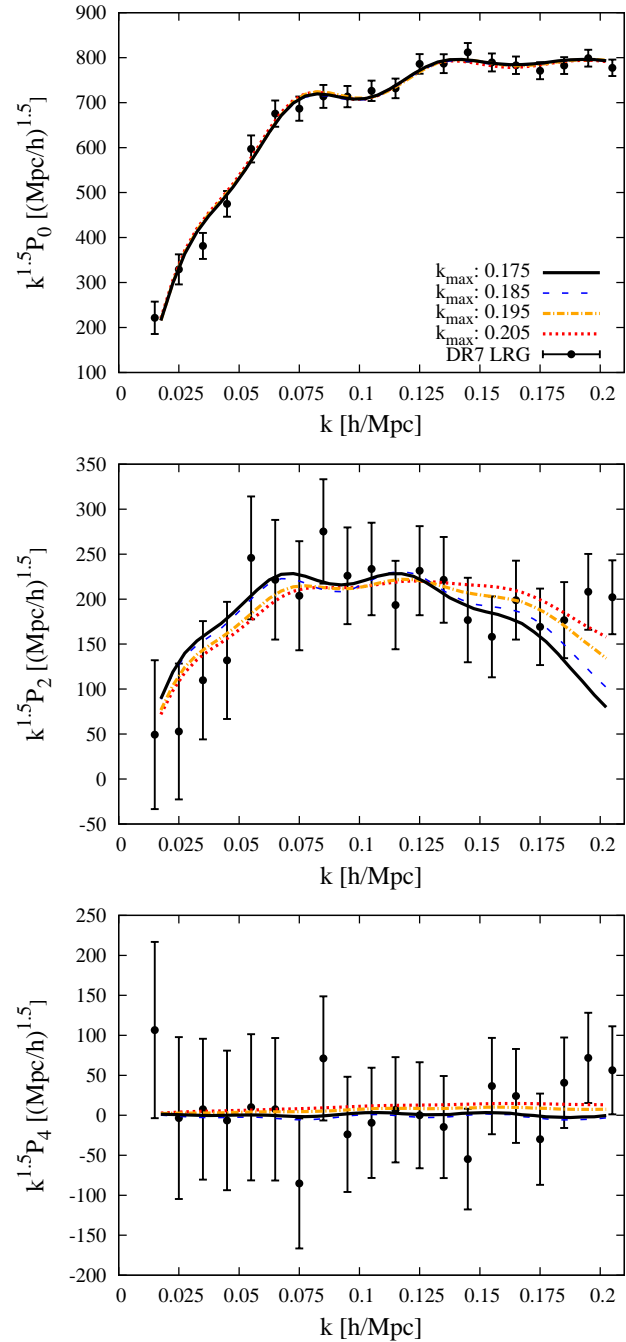


Figure 10. Comparisons of the best-fitting curves with the SDSS DR7 LRG sample with different k_{\max} from 0.175 to 0.205 [h/Mpc]. We plot the best-fitting curves with $k_{\max} = 0.175$ [h/Mpc] in solid, $k_{\max} = 0.185$ [h/Mpc] in (blue; colors are available for the online version) dashed, $k_{\max} = 0.195$ [h/Mpc] in (orange) dot-dashed, and $k_{\max} = 0.205$ [h/Mpc] in (red) dotted line. We also plot the measured multipole power spectra of the SDSS DR7 LRG sample in filled circles.

Author	Sample	Measurement	Redshift	Galaxy bias	$f(z)\sigma_8(z)$	$D_A(z)$ [Mpc]	$H(z)$ [Mpc/km/s]
This work	SDSS DR7 LRG	P_0, P_2, P_4	0.3	$b_0(1 + A_2k^2)/(1 + A_1k)$	$0.49 \pm_{stat.} 0.08 \pm_{sys.} 0.04$ ($f = 0.71 \pm_{stat.} 0.12 \pm_{sys.} 0.06$)	$968 \pm_{stat.} 42 \pm_{sys.} 17$	$81.7 \pm_{stat.} 5.0 \pm_{sys.} 3.7$
Samushia et al. (2012)	SDSS DR7 LRG	ξ_0, ξ_2	0.25 0.37	constant (fix) constant (fix)	0.35 ± 0.06 0.46 ± 0.04	- -	- -
Xu et al. (2013)	SDSS DR7 LRG	ξ_0, ξ_2	0.35	constant (fix)	-	1050 ± 38	84.4 ± 7.1
	SDSS DR7 LRG	$P(k, \mu)$	0.35	constant (float)	-	1050 ± 38	84.4 ± 7.1
Reid et al. (2012a)	BOSS CMASS	ξ_0, ξ_2	0.57	constant (float)	0.43 ± 0.069	2190 ± 61	92.4 ± 4.5
Blake et al. (2011b)	WiggleZ	P_0, P_2	0.22 0.41 0.6 0.78	constant (float)	0.42 ± 0.07 0.45 ± 0.04 0.43 ± 0.04 0.38 ± 0.04	- - - -	- - - -
Contreras et al. (2013)	WiggleZ	ξ_0, ξ_2	0.2 0.4 0.6 0.76	constant (float)	0.50 ± 0.14 0.40 ± 0.06 0.37 ± 0.08 0.42 ± 0.09	- - - -	- - - -

Table 2. Comparison with previous works. Note that the normalization factor, $\sigma_8(z = 0.3) = 0.696$, is fixed throughout this work. Let us emphasize that we put the simultaneous constraints on f , D_A , and H .